Nanoscale

REVIEW

View Article Online
View Journal | View Issue

Cite this: *Nanoscale*, 2026, **18**, 2916

Light outcoupling strategies for quantum dot light-emitting diodes

Rakesh Kumar Jha,[a,c] Hyuntai Kim [b] and Seong-Yong Cho *[c]

Quantum dot LEDs (QLEDs) combine exceptional colour purity, narrow emission linewidths, and tunable spectral properties, establishing them as front-runners for next-generation displays and lighting technologies. Despite significant advancements in material and device engineering, their external quantum efficiency remains intrinsically constrained by inefficient light outcoupling (LOC), with a substantial portion of emitted photons trapped by total internal reflection, waveguide confinement, and metallic absorption. These optical losses should be confronted head-on to envision a breakthrough in the suboptimal performances of the contemporary QLEDs. Herein, we launch a plethora of advanced strategies to discuss mitigative approaches for critically analysing and improving the LOC discrepancies in QLEDs. The LOC strategies, rigorously evaluated in our study, include microcavity engineering, refractive index modulation, dipole orientation control, and surface/interface engineering. Each strategy is examined in terms of its physical basis, design principles, fabrication complexities, and trade-offs in device performance. Special attention is given to enhancing light extraction while maintaining angular emission uniformity, structural stability, and scalability for large-scale manufacturing. Collectively, our LOC strategies delineate a clear roadmap toward the development of high-efficiency, commercially viable QLEDs for advanced optoelectronic applications.

Received 26th July 2025,
Accepted 7th January 2026

DOI: 10.1039/d5nr03160e

rsc.li/nanoscale

1. Introduction

Light-emitting diodes (LEDs) underpin modern optoelectronics, valued for their exceptional efficiency, longevity, compactness, and ultrafast modulation, which collectively enable a broad spectrum of applications spanning general illumination, display technologies, optical communication, and

[a]*Department of Electronic Engineering, Hanyang University, Seoul 04763, Korea*
[b]*Department of Electrical and Electronic Convergence Engineering, Hongik University, Sejong 30016, Korea*
[c]*Department of Photonics and Nanoelectronics, BK21 FOUR ERICA-ACE Centre, Hanyang University ERICA, Ansan 15588, Korea.*
E-mail: seongyongcho@hanyang.ac.kr

Rakesh Kumar Jha

Rakesh Kumar Jha received the M.S. degree from the School of Electronics Engineering, Kyungpook National University (KNU), Daegu, Korea, in 2016. He then served as a researcher in Sejong University and Ajou University where he engineered biomedical/biomaterial optical devices. He is currently a fourth-year Ph.D. degree candidate at the Department of Electronic Engineering, Hanyang University, Seoul, Korea. His research focuses on optical simulation, device fabrication, and characterization of cadmium-free standard and inverted TE-QLED devices for display applications.

Hyuntai Kim

Hyuntai Kim received the Ph.D. degree from the School of Electrical Engineering, Seoul National University (SNU), Seoul, Korea, in 2016. He subsequently held a Postdoctoral Fellowship at SNU, for one year. He joined the Optoelectronics Research Centre (ORC), University of Southampton, as a Research Fellow, in 2017. Since 2019, he has been with the Department of Electrical and Electronic Convergence Engineering, Hongik University, Sejong, as an Associate Professor. He is primarily interested in fibre optics, nanophotonics, and artificial intelligence. He has authored/co-authored over 30 original research publications.

biomedical instrumentation.[1] Among these, colloidal quantum dot light-emitting diodes (cQLEDs) have emerged as a transformative platform, fundamentally redefining the landscape of solid-state lighting and display engineering. The remarkable evolution of cQLEDs is driven by their unparalleled colour purity, highly tuneable emission profiles, robust structural stability, and compatibility with solution-processable fabrication schemes amenable to large-area and flexible integration.[2–7] Continued refinement of core/shell nanocrystal architectures and surface passivation techniques has yielded quantum dots (QDs) exhibiting near-unity photoluminescence quantum yields (PLQYs) with spectrally narrow emission, translating into external quantum efficiencies (EQEs) exceeding 25% and luminance surpassing 10^5 cd m^{-2} for red and green devices. Rapid progress in indium phosphide (InP)-based systems has likewise delivered EQEs approaching 20% establishing a viable cadmium-free alternative for environmentally sustainable optoelectronics.[8–17] Meanwhile, iterative improvements in colloidal synthesis, including hot-injection protocols and anisotropic nanocrystal growth, have further enhanced monodispersity, spectral stability, and operational durability, positioning cQLEDs as front-runners for next-generation emissive devices.[18–20]

Despite these significant advances in material design and charge-transport engineering, the overall performance of QLEDs remains fundamentally constrained by their intrinsically limited external light extraction efficiency (LEE).[21–24] While QDs can achieve internal PLQYs approaching the theoretical maximum of 100%, only a fraction of the internally generated photons—typically 20–30%—successfully escape the layered device architecture into free space. This severe optical bottleneck originates from a series of intertwined loss mechanisms, including total internal reflection (TIR) at high refractive-index (RI) device interfaces, photon confinement within waveguide and substrate modes, reabsorption by optically lossy charge transport layers (CTLs) or metallic contacts, and anisotropic dipole orientations that restrict efficient outcoupling along the surface normal.

Conceptually, the emission in QLEDs may be envisioned as photon generation occurring within a nanoscale optical cavity in which a significant portion of emitted photons become trapped as guided or evanescent modes unable to surpass the critical angle at the semiconductor-air interface. These trapped photons undergo repeated internal reflections or non-radiative absorption, dissipating as heat rather than contributing to observable luminance. Consequently, even as the internal quantum efficiency (IQE) approaches its fundamental limit, the EQE and practical luminance remain severely limited by this extraction inefficiency. Overcoming such limitations necessitates a holistic optical design perspective, encompassing both field manipulation and material integration, to reconcile internal emission potential with external radiative performance.[25–27]

Recent research efforts have therefore focused on comprehensive light outcoupling (LOC) strategies that integrate photonic and electronic optimization to mitigate confinement losses. Patterned substrates, quasi-periodic photonic crystals, and tailored RI matching layers effectively perturb guided modes and alleviate TIR-induced confinement.[28–30] Concurrently, deliberate alignment of QD transition dipoles—achieved through ligand engineering, anisotropic nanocrystal morphology, and matrix-assisted orientation control—has proven instrumental in promoting horizontal dipole orientation, thereby enhancing vertical LOC efficiency.[31–34] Furthermore, microcavity (MC)-engineered top-emitting (TE) configurations have been shown to refine the internal field distribution, enabling directional emission, enhanced luminance uniformity, and colour stabilization.[35–37] When combined with advanced CTL designs, such as doped electron injection layers and composite hole transport architectures, these optical and electrical strategies jointly reinforce carrier balance and emission robustness.[38–41] The convergence of optical field control and balanced electronic transport thus remains a central paradigm for bridging the persistent gap between idealized IQEs and achievable EQEs in high-performance QLEDs.[42,43]

The ongoing transition toward cadmium-free QLED systems based on InP and zinc selenide telluride (ZnSeTe) further complicates optical optimization, as differences in RI contrast, dipole anisotropy, and surface chemistry introduce additional challenges for light extraction.[44–47] Simultaneously, the rise of flexible and stretchable display architectures demands mechanical resilience, necessitating that emissive and optical layers maintain their optical coherence, interfacial integrity, and emission stability under mechanical stress.[48–50] Despite substantial progress in environmental passivation—through encapsulation, cross-linked ligand matrices, and chemically robust core–shell configurations—device longevity remains constrained by photooxidation, trap-induced non-radiative recombination, and ion migration.[51–56] Hence, continued refinement of CTL energetics and molecular design to balance

Seong-Yong Cho

Seong-Yong Cho received the Ph. D. degree from the department of Materials Science and Engineering, SNU, Seoul, Korea, in 2015. He pursued a Postdoctoral Research Associate Position at University of Illinois at Urbana-Champaign, IL, USA, until 2017. From 2018, he served as an Assistant/Associate Professor at the Department of Materials Science and Engineering, Myongji University, Yongin, Korea. From 2023, he has been affiliated as an Associate Professor with the Department of Photonics and Nanoelectronics, Hanyang University ERICA, Ansan, Korea. His research focuses on applications of nanomaterials and QDs for display technologies. He has authored/co-authored over 50 original research publications.

carrier injection while suppressing exciton-driven degradation remains imperative for long-term operational stability.[57]

To this end, this review systematically elucidates the optical, material, and structural principles underpinning efficient LOC in QLEDs. It dissects the dominant loss channels—waveguide, plasmonic, and absorptive—through quantitative optical modelling, while contextualizing state-of-the-art LOC strategies spanning RI modulation, dipole orientation engineering, and MC or nanoarchitectured photonic structures. Building upon these foundations, it further explores emerging design frameworks that integrate electronic charge equilibrium, optical field management, and mechanical stability toward holistic performance optimization.

Crucially, this discourse seeks to delineate the key scientific questions that define the frontier of LOC research in QLEDs. Foremost among these is how the relative contributions and interactions of distinct optical loss mechanisms—waveguiding, SPP dissipation, and absorption quenching—can be quantitatively resolved across varied device architectures to enable predictive modelling of extraction-limited efficiencies. A second key question concerns which conceptual and structural strategies can facilitate the cooperative integration of multiple photonic design elements, including RI modulation, dipole orientation control, and resonant MC engineering, while preserving spectral fidelity, charge balance, and operational stability. Finally, it remains crucial to understand how these photonic–electronic paradigms may be extended to mechanically deformable and cadmium-free material systems without compromising emission uniformity or device longevity. Addressing these questions requires the establishment of an integrative framework that unifies nanoscale optical physics, material chemistry, and device engineering—an aspiration now increasingly attainable through systematic elucidation of QLED optical loss channels.

2. QLEDs

QLEDs have emerged as a paragon of modern electroluminescent (EL) technology, embodying the convergence of nanoscience precision and optoelectronic functionality. Their ascendancy stems from the exceptional attributes of cQDs—size-tuneable bandgaps, near-unity PLQYs, and spectrally pure emission—attributes that collectively transcend the limitations of conventional emissive semiconductors. The evolution of QLEDs has not been a linear progression, but rather a mosaic of interdependent breakthroughs across materials chemistry, interface engineering, and device architecture. This trajectory, schematically illustrated in Fig. 1, delineates the sequential milestones (highlighted in cyan) that have propelled QLEDs from laboratory curiosities to commercially pertinent contenders, alongside the steady ascension in their LOC efficiencies (highlighted in yellow). The following subsections articulate this development chronologically and thematically—from molecular and interfacial design principles to band alignment strategies and architectural innovations—thereby tracing the intricate nexus between scientific insight and technological realization.

2.1 Materials and device engineering in QLEDs

At the heart of QLED advancement lies the perpetual refinement of material systems. The rational design of QD core/shell heterostructures, guided by the principles of strain management, band-edge control, and surface passivation, has driven PLQYs to the brink of unity.[58–61] Simultaneously, the transition from cadmium-based to environmentally benign, heavy-metal-free compositions (*e.g.*, InP, ZnSe, and ZnTe) underscores a paradigm shift: the alignment of ecological sustainability with optoelectronic excellence.[62–67] Beyond the intrinsic QD chemistry, the optimization of surrounding CTLs has emerged as an equally vital dimension. Through the deliberate engineering of carrier energy levels and mobilities, these layers orchestrate balanced carrier injection, suppress interfacial trap formation, and minimize non-radiative losses—culminating in substantially reduced driving voltages and extended operational stability.[68–72]

Parallel to electronic optimization, optical MC engineering has evolved into a defining strategy for pushing QLED performance boundaries. The deliberate tuning of cavity resonance conditions enables spectral narrowing, colour enhancement, and luminance amplification—key attributes for next-generation ultra-high-resolution displays and augmented reality (AR) microdisplays.[73] Yet, the pursuit of perfection in QLEDs is as much about endurance as efficiency. Degradation phenomena driven by oxygen, moisture, heat, and bias-induced ion migration persist as formidable obstacles to long-lived operation. Addressing these vulnerabilities, the advent of inorganic encapsulation barriers, atomic-layer-deposited ultrathin passivation layers, and thermally robust matrix architectures have extended device lifetimes to operationally relevant regimes.[74–80]

Equally transformative are the parallel strides in process and integration technologies. Continuous-flow and microreactor-assisted QD syntheses have assured compositional uniformity at industrial scales, while ink formulation and printing protocols have enabled impeccable film homogeneity and interpixel consistency. As such, materials innovation and process engineering are now inseparable pillars—the former defining the quantum limits of emissive performance, and the latter dictating their translation into manufacturing reality.[81–84] These foundational advances naturally segue into the next critical consideration: how these materials interface energetically within the multilayer QLED stack to enable efficient carrier recombination—a domain encapsulated by energy band alignment.

2.2 Energy band alignment in QLEDs

The operational physics of QLEDs is governed by the choreography of electrons and holes within an energy landscape meticulously sculpted across interfaces. Radiative recombination within the QD emission layer (EML) occurs only when these carriers are injected, confined, and balanced with near-atomic precision. Thus, energy band alignment serves as the electrostatic blueprint dictating the flow, accumulation, and recombination of charge carriers—a subtle yet decisive determinant of quantum efficiency and luminance stability (Fig. 2).

Fig. 1 Milestones in the evolution of QLEDs (cyan colour background) and advancements in LOC efficiency of QLEDs (yellow colour background).

On the electron injection side, low-work-function metals such as Al ($\Phi \approx 4.1$ eV) and Ag ($\Phi \approx 4.3$–4.7 eV) establish intimate contact with zinc oxide (ZnO) or its magnesium-alloyed derivatives (ZnMgO), presenting minimal injection barriers (<0.2 eV).[85] The introduction of Mg not only expands the bandgap and modulates the electron affinity (~4.0 eV) but also suppresses parasitic ETL absorption, an often-overlooked yet critical factor for preserving luminous efficacy.[86] The ETL/QD interface, in turn, must negotiate a delicate equilibrium: an offset of approximately 0–0.3 eV ensures electron confinement within the EML without inducing excessive charge accumulation at the heterointerface. For blue-emitting ZnSeTe QDs, such offsets approach zero; conversely, red-emitting InP cores often necessitate interfacial dipole engineering—typically *via* polyethyleneimine surface modification—to reconcile misaligned bands.[87]

On the hole injection side, transparent anodes such as indium tin oxide (ITO, $\Phi \approx 4.7$–5.1 eV) or reflective Ag/molybdenum trioxide (MoO_3) composites must align seamlessly with high-work-function hole-injection materials. PEDOT:PSS ($\Phi \approx$

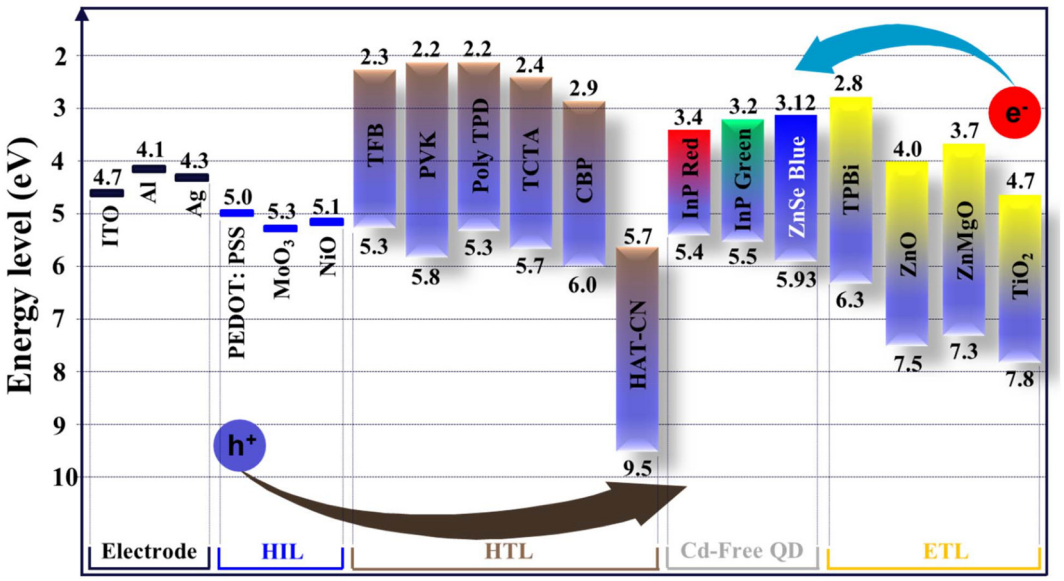

Fig. 2 Energy band diagrams for Cd-free QLED components.

5.0 eV) suits moderate band requirements, while MoO_3 ($\Phi \approx$ 5.3 eV) affords deeper alignment for high-barrier configurations.[88,89] These cascaded interfaces facilitate hole injection barriers below 0.3 eV and blockade electron backflow. The subsequent HTL/QD interface, frequently employing polymers such as TFB or Poly-TPD (HOMO $\approx$ 5.3 eV), imposes a gentle energetic descent toward the QD valence band (VB $\approx$ 5.4 eV), ensuring exciton confinement.[90] For wide-bandgap blue QDs, deeper HOMO materials like CBP (HOMO $\approx$ 6.0 eV) are strategically deployed to alleviate leakage currents and suppress quenching through triplet–triplet annihilation.[91]

This intricate electronic alignment establishes a harmonious energy landscape where charge carriers converge and recombine radiatively with minimal loss. Building upon this energetic architecture, QLED design transitions to its ultimate dimension—device architecture—where physical structure and optical resonance are integrated to extract the full measure of quantum efficiency from the engineered energy landscape.

2.3 Architectural innovations and commercial prospects

The evolutionary frontier of QLEDs now lies in the architectural orchestration of optical and electronic design principles. Device configuration—whether bottom-emitting (BE) or TE—exerts profound influence over both photon management and integration viability (Fig. 3). BE-QLEDs, inheriting the straightforward geometry of their organic LED (OLED) predecessors, offer fabrication simplicity but suffer from substrate-related waveguiding and optical trapping.[92–95] In contrast, TE-QLEDs,

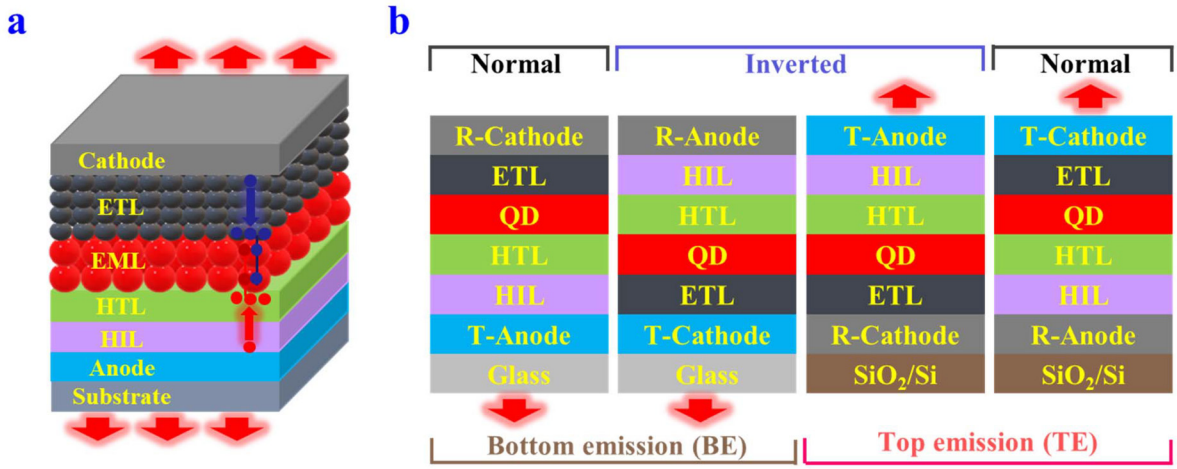

Fig. 3 QLED device architectures. (a) Schematic configuration for contemporary QLEDs. (b) Standard and inverted designs for both BE- and TE-QLED structures.

by harnessing MC engineering, transcend these optical constraints. The coupling of metallic reflectors and optical resonances facilitates intensified field confinement, directional emission, and linewidth contraction—features indispensable for micro-display technologies and wafer-level monolithic integration on opaque substrates.[96–107]

As the field has matured, the performance of QLEDs has entered a new competitive echelon: EQEs surpassing 29% for green cadmium selenide (CdSe)-based devices and approaching 15% for heavy-metal-free InP systems, accompanied by operational lifetimes exceeding 10^3 hours at 1000 cd m^{-2}. Yet, despite such strides, the path to full-scale commercialization remains defined by the persistence of several scientific crucibles—the stabilization of blue-emitting QDs, defect-neutral interface formation, and the synergistic tuning of charge mobility and surface passivation.[108–110]

To surmount these constraints, the discipline increasingly embraces multi-shell nanocrystal architectures, atomic-level interface design, and vertically integrated fabrication workflows that merge optical, chemical, and electronic optimization within a single framework. These developments collectively signal a paradigm transition: QLED research is no longer merely about improving individual metrics, but rather about achieving systemic harmony between quantum structures and macroscopic device realities. As such, QLEDs now stand poised at the confluence of fundamental science and industrial scalability, signifying not merely the evolution of a display technology, but the maturation of a quantum-engineered emissive platform underpinning the future of visual electronics.

3. Dominant optical channel loss pathways in QLEDs

Optical channel losses in QLEDs represent a multifaceted challenge impacting device efficiency and operational stability. The photons generated in the QD EML manifest in several optical channels. Only those coupled into the air mode escape the device, directly contributing to visible emission and EQE. Significant fractions, however, are lost to waveguides, surface plasmon polaritons (SPPs), and absorption/interference, all of which must be overcome to advance QLED performances.

3.1 Optical loss mechanisms in QLEDs

In QLED device architectures, waveguide modes emerge due to the high RI contrast between the QD layer, ETL, and semi-transparent metallic cathode *versus* the surrounding media. Photons entering these waveguide channels are confined by TIR, trapped within the device stack, and ultimately dissipated as heat rather than emitted, resulting in reduced brightness and efficacy. The degree of trapping scales with RI mismatch and device geometry, thus requiring precise control in engineering the layer composition and thickness.

At the interface of the QD EML and metallic cathode or anode, electromagnetic fields can couple to free electrons, forming SPPs, thereby converting optical energy into collective electron oscillations. The energy is rapidly dissipated as heat, contributing substantially to optical losses, local heating, and potential chemical degradation of materials near electrodes.[103]

Minimizing SPP losses relies on careful spatial and dielectric separation of the EML and metal contacts. Reducing SPP loss relies on several strategies: by either choosing thinner or less "lossy" metals, or adding extra thin layers to separate light from metal surfaces. Aligning the QDs so their light doesn't get trapped by the metal can also help. Careful design of the device layers (like using special thicknesses and patterns) can guide light to escape. Some advanced techniques even try to recover this lost energy by redirecting it back out as useful light, using tiny surface patterns or special layer arrangements.[111,112] However, it's important to balance these strategies—sometimes making a change to improve LOC can make electrical performance worse, or make the device harder to build and keep stable. The best results come from a combination of methods, carefully tailored for both optical and electrical performance, so more of the generated light exits the device without sacrificing reliability or efficiency.

Device layers designed for charge transport, such as ITO, PEDOT:PSS, and ETLs, can absorb a portion of the internally generated photons. This optical absorption transforms what could contribute to the device's visible output into heat, limiting EQE and aggravating the thermal budget of the device. Additionally, interference effects associated with non-ideal thicknesses and RI mismatches in the cavity can suppress emission along the normal direction. This is particularly detrimental to display applications where directional brightness and narrow angular colour shifts are required.

3.2 Managing optical losses in QLEDs

The compounded optical channel losses decrease EQE, colour purity, and ultimately operational lifetimes of QLEDs. The trapping and conversion of photons within the device, whether into waveguide or SPP modes, or lost through absorption/interference, imposes not only photonic inefficiency but also thermal stress, accelerating both chemical and structural degradation within the device architecture. Advancing QLED technology toward commercialization necessitates a rigorous understanding and effective management of optical channel losses, which critically limit device efficiency and brightness. Effective commercialization demands integration of advanced optical modelling, nanophotonic design, and materials innovation.

Central to this effort is implementing multidisciplinary LOC strategies that emphasize precise control of multilayer thicknesses, tailored RI engineering, and optimizing antinode alignment with emission wavelengths to maximize constructive interference at the air interface. Implementation of sophisticated nanophotonic architectures such as microlens arrays, scattering layers, and photonic crystals enables the redirection of photons otherwise trapped in waveguide and SPP modes into the air mode, thereby significantly enhancing LEE. Complementary use of dielectric spacers and engineered interfaces suppresses SPP formation, which otherwise converts

useful optical energy into thermal losses and deteriorates device stability.

Optimizing the thickness of the ITO interlayer in TE-QLEDs plays a critical role in resolving dominant optical loss mechanisms and enhancing device performance. When the ITO thickness is minimized to around 2 nanometres, the air mode, which corresponds to photons escaping the device, constitutes approximately 29.4% of the total emitted optical power, thereby significantly improving LEE (Fig. 4a). However, increasing the ITO layer thickness to approximately 90 nanometres drastically diminishes this air mode contribution to about 3.7%, concurrently increasing the strength of waveguide modes that trap photons within the device layers (Fig. 4b). This redistribution results in reduced luminous efficiency due to enhanced photon confinement. Experimental power-dissipation spectra provide further evidence, with the number of waveguide modes increasing from three to four as the ITO thickness grows from 5 nm to 80 nm, indicating destructive interference within the MC that suppresses essential on-axis emission needed for directional luminance and colour fidelity (Fig. 4c). Complementary wavelength-resolved power maps demonstrate that an ITO thickness near 5 nm strikes an optimal balance by minimizing waveguide and SPP losses, yielding LOC efficiency near 30% at the 627 nm resonance, the highest value among substrates tested (Fig. 4d–f). The congruence between simulation and experiment highlights the necessity for precise optical MC engineering with ultrathin ITO layers that not only bolster constructive interference for enhanced light output but also maintain favourable electrical characteristics. This refined design strategy effectively mitigates intrinsic waveguide and plasmonic losses, providing a foundational approach for advancing TE-QLED architectures aimed at achieving high luminance and spectral purity in state-of-the-art, high-resolution display and lighting technologies.

4. Strategies to rationalize LOC in QLEDs

Engineering efficient LOC in QLEDs necessitates an intricate balance between optical field control, electronic integrity, and process compatibility. LOC strategies are broadly categorized as intrinsic and extrinsic, depending on whether the optimization is embedded within the device stack or externally applied after fabrication. Intrinsic LOC strategies—such as MC tuning, horizontal-dipole engineering, and the integration of embedded photonic structures—are implemented during

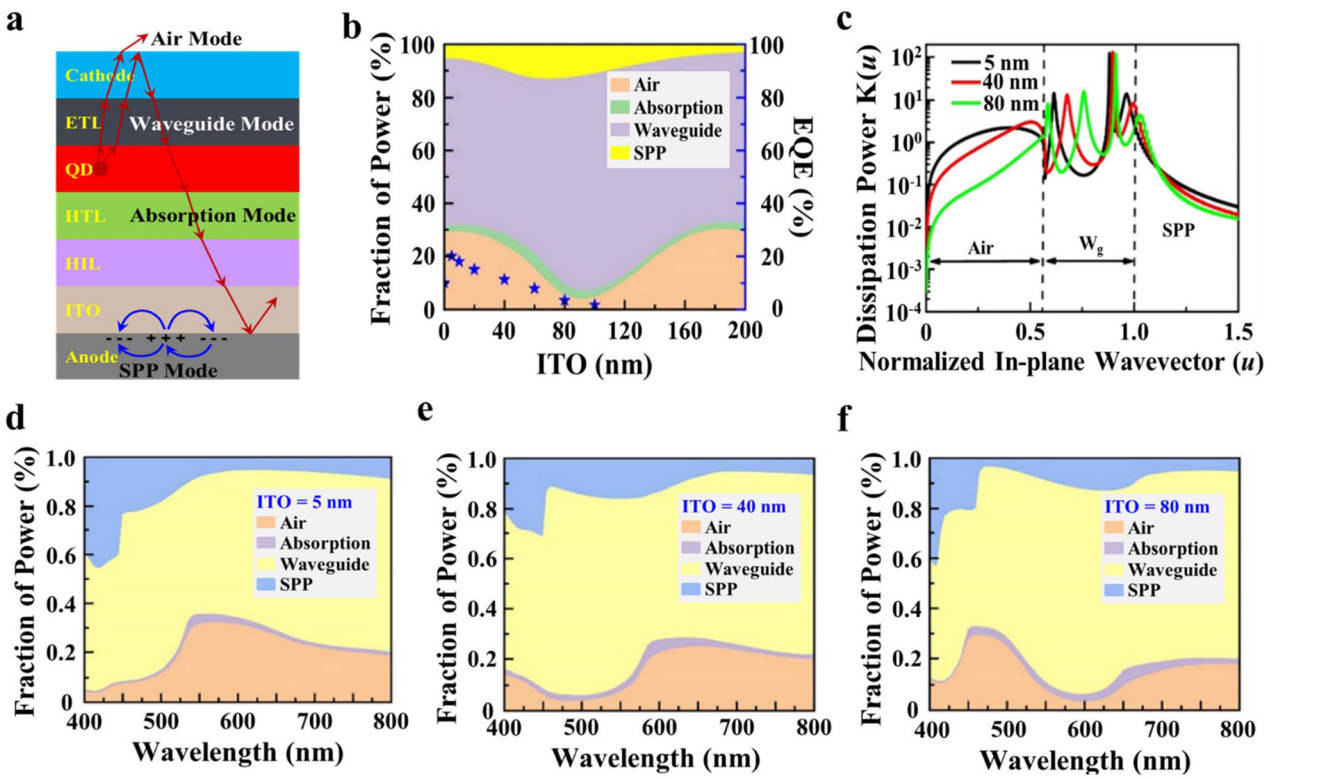

Fig. 4 Optical channels in TE-QLED devices. (a) Schematic diagram of optical channels with TE-QLEDs. (b) Changing the proportions of different optical channels by tuning the ITO interlayer thickness for the TE-QLEDs by the SETFOS software. In addition, the experimental data of TE-QLEDs are compared with the simulation results of the device. (c) Power dissipation spectra at λ = 627 nm of devices. The wavelength-dependent optical power distribution of the TE-QLEDs with (d) 5 nm, (e) 40 nm and (f) 80 nm ITO interlayer. ((b)–(f) Reprinted with permission from ref. 113. Copyright 2024 Royal Society of Chemistry).

wafer-level fabrication. These approaches can simultaneously enhance both device efficiency and colour purity. However, they also demand careful alignment between optical and electrical properties to avoid performance trade-offs. In contrast, extrinsic methods—including microlens arrays, diffuse scattering films, and other macro-optical elements—are typically applied after device fabrication. Although these techniques impose fewer process constraints and effectively deliver broadband luminance gains, they often come at the cost of increased device thickness and manufacturing expense (Fig. 5). When judiciously integrated, these intrinsic and extrinsic architectures improve LOC in QLEDs by reshaping where and how photons are generated and guided, ultimately enabling more of them to escape into air.

At the physical level, these enhancements arise from precise control over the optical environment surrounding the QDs. MC engineering employs reflective electrodes and optimized layer thicknesses to position QDs at optical antinodes, thereby reinforcing forward emission and narrowing the emission spectrum. RI tuning further mitigates TIR and SPP losses by moderating index contrast and distancing QDs from lossy metallic layers. Dipole orientation control provides another degree of optimization, aligning QD transition dipoles preferentially out of plane to suppress coupling into lateral waveguide and plasmonic modes. Finally, surface/interface engineering through nanostructures or microlens arrays redirects guided photons into the escape cone by scattering or refraction, effectively converting trapped optical modes into useful far-field emission. The subsequent sections provide an in-depth treatment of each of these LOC mechanisms—namely MC engineering, RI tuning, dipole orientation control, and surface/interface engineering—detailing how they can be systematically integrated to maximize optical extraction in QLEDs.

4.1 MC engineering

MC engineering stands as a foundational pillar among intrinsic LOC strategies for QLEDs, harnessing resonant optical interference to systematically suppress the dominant loss channels that limit device efficiency. By confining spontaneous emission within precisely tuned reflective boundaries, MC design transforms broadband, multidirectional photon generation into spectrally and angularly selective radiation, thereby elevating the proportion of light that escapes the device stack into useful far-field emission.

4.1.1 Optimization of MC for optical loss mitigation. MC engineering mitigates the multifaceted optical losses in QLEDs by transforming spontaneous emission into cavity-selected,

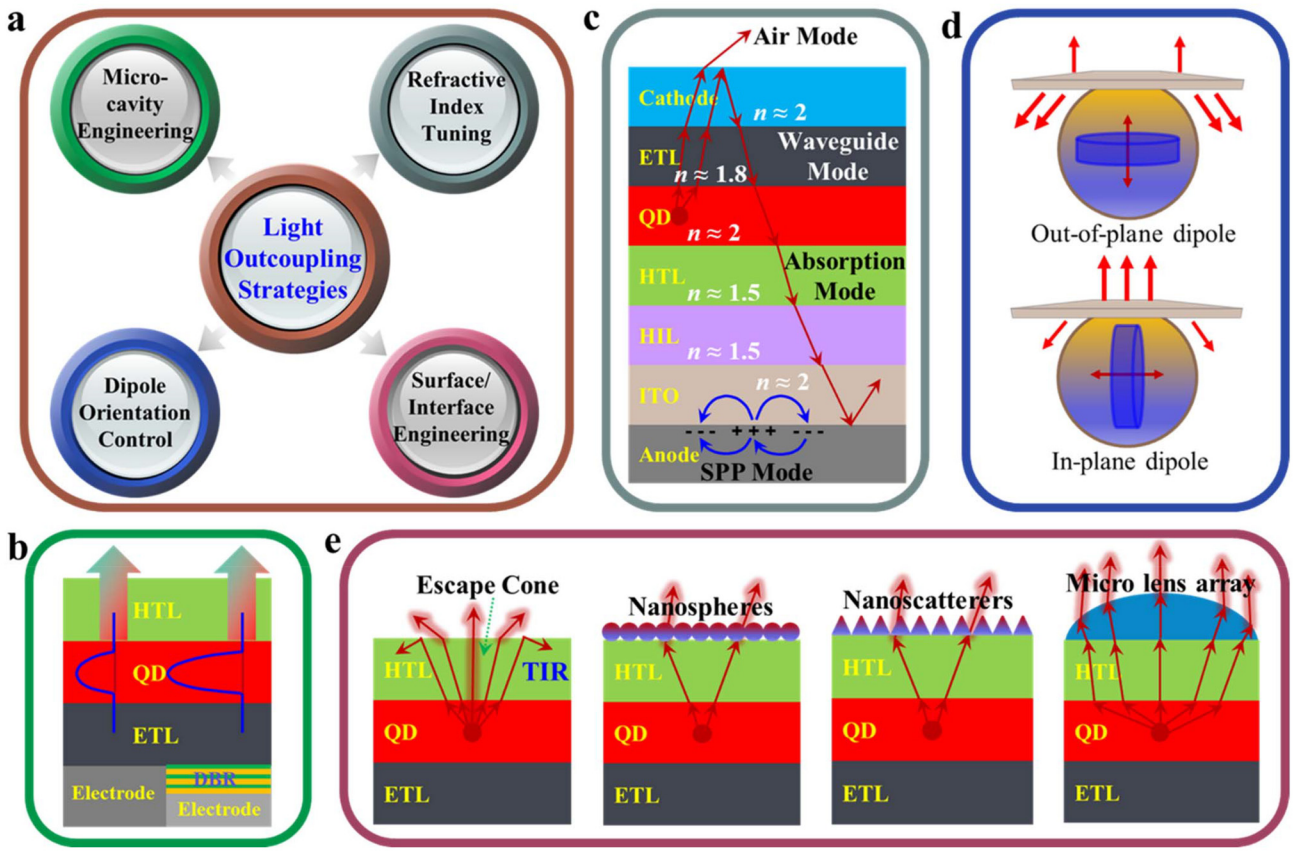

Fig. 5 LOC strategies for QLEDs. (a) Key strategies employed in this work. (b) MC engineering. (c) RI tuning. (d) Dipole orientation control. (e) Surface/interface engineering.

highly directed radiation that satisfies specific resonance conditions. When the QD recombination zone is precisely positioned at an antinode within a cavity bounded by partially reflecting electrodes, the standing optical field selectively amplifies near-normal modes while attenuating off-resonant, laterally propagating ones that otherwise feed waveguide, SPP, or parasitically absorbed channels. This spectral–angular filtering redistributes the emitted photon flux toward outcoupled radiative modes, yielding marked gains in light extraction, emission directionality, and spectral purity without materially altering the underlying charge-transport landscape.

Notwithstanding these benefits, MC design is intrinsically a multi-objective optimization problem demanding a careful equilibrium between optical enhancement and electrical integrity—a balance that extends naturally from the field's selective amplification to practical device engineering. The resonant cavity thickness that maximizes extraction efficiency or colour saturation may not necessarily coincide with the optimal distance for charge injection or transport, introducing design trade-offs that must be rationally reconciled through complementary strategies. Targeted mitigation thus aligns waveguide losses with detuned CTL thicknesses, SPP coupling with extended QD-metal spacing *via* low-index atomic layer deposition (ALD) interlayers (*e.g.*, Al_2O_3), and absorption with phase-optimized electrode reflectivities, ensuring photonic gains reinforce rather than conflict with electrical function. This interplay underscores the MC concept's broad versatility across emissive technologies—from perovskite LEDs (PeLEDs) to QLEDs—owing to their narrow intrinsic linewidths and high RIs, which inherently harmonize with resonant cavity effects to amplify constructive interference (Fig. 6a).

Such versatility, however, confronts a recurring challenge: angular colour dispersion, arising as an unavoidable consequence of wavelength-dependent phase accumulation that subtly perturbs the very field selectivity enabling MC benefits. Emission angle-dependent chromatic shifts compromise viewing uniformity, yet they can be alleviated through angular redistribution layers or low-haze scattering films that extend the cavity's directional control into broader angular regimes. Despite this added layer of refinement, the MC framework endures as one of the most powerful and experimentally validated routes toward achieving concurrent improvements in optical extraction, chromatic stability, and spectral narrowing, particularly when its photonic precision is coherently coupled with the device's electrical architecture.[113–115]

This coupled design philosophy finds concrete expression in Fig. 6b, which illustrates the MC optimization strategy essential for achieving high-efficiency TE-QLEDs and builds directly on the interplay of field positioning and loss mitigation. The first step involves fine-tuning thicknesses of the semi-transparent top electrode and surrounding CTLs to modulate wide-angle interference and multi-beam effects, thereby extending antinode precision across the device stack. Complementing this, employing an ultrathin EML becomes critical—not only to confine excitonic dipoles at the cavity antinode but also to minimize optical reabsorption that could otherwise erode interference contrast—revealing how structural subtlety sustains the framework's photonic advantages. Prior studies[116,117] have illuminated the profound benefits of such thin EMLs, enhancing both optical coherence and electrical balance in ways that echo the broader MC equilibrium.

These structural refinements, in turn, unlock MC effects that transcend LEE, profoundly influencing the emitter's intrinsic quantum yield through the Purcell effect—a natural progression from cavity field control to modified local density of optical states. A properly engineered cavity accelerates radiative decay for in-plane (horizontal) dipoles while suppressing out-of-plane (vertical) ones, yielding anisotropic enhancement whose significance lies in elevating overall radiative efficiency. By favouring modes that couple effectively into free space, the dipole selectivity further diminishes losses to SPPs and waveguide channels, seamlessly integrating the cavity's angular and spectral mastery into fundamental emission physics.[118]

4.1.2 Fundamental strategies in MC engineering. Building directly on these optimization principles, LOC strategies predicated on MC engineering have solidified as a cornerstone for

a

Requirements	Effects	MC Strategy
Material	Emission spectrum	Narrower is better
Device	EML thickness	Thin
	Absorption	Low
	CTL thickness	Resonance matching
Optical	Effects	MC effect
		Purcell effect
	LEE limit	20–50 %
	Angular distribution	Non-Lambertian
Difficulty		Thickness control

b

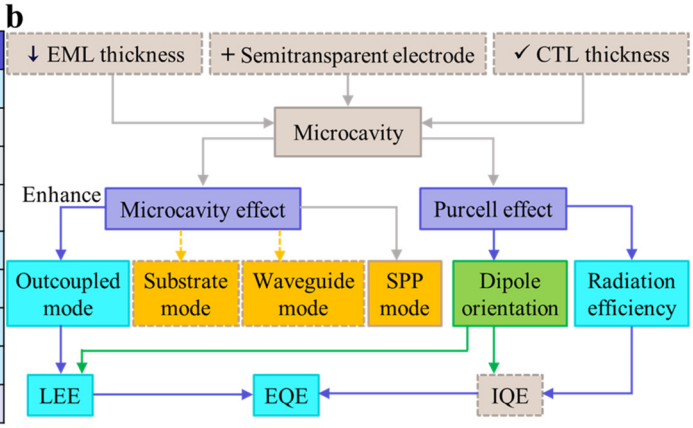

Fig. 6 Optimization of MC in TE-QLEDs. (a) Requirements for and effects of the MC engineering. (b) Flow diagram for MC optimization in QLEDs.

elevating optical performances across light-emitting devices, including PeLEDs, OLEDs, and QLEDs. In this paradigm, MC engineering harnesses fundamental optical interference within a meticulously configured Fabry–Pérot (FP) cavity, wherein the QD EML is symmetrically flanked by highly reflective surfaces—typically a metallic bottom mirror (R > 95%) and dielectric/metal hybrid top coupler—forming a vertical resonator. Resonance occurs when the round-trip optical path length of the cavity equals an integer multiple of the emission wavelength, fostering constructive interference that amplifies on-axis spectral radiance while directing emission along the cavity axis.[119]

Theoretical and empirical investigations distinguish two primary classes of optical interference that underpin MC devices: multiple-beam interference (MBI) arising from multilayer reflections and FP resonance (FPR) characteristic of etalon structures.[120,121] By systematically adjusting cavity length, RI, and phase shift parameters, robust constructive interference can be achieved at targeted wavelengths with the resonance condition formally captured by the equation governing phase accumulation across the structure, as articulated below.

$$\frac{2\pi}{\lambda}2nd_1\cos\theta + \phi_{\text{bottom}} = m_1 2\pi \quad (1)$$

$$\frac{2\pi}{\lambda}2n(d_1 + d_2)\cos\theta + (\phi_{\text{bottom}} + \phi_{\text{top}}) = m_2 2\pi \quad (2)$$

These equations incorporate the free-space wavelength (λ), angularly averaged RI (n), emitter-to-electrode distances (d_1, d_2), emission angle (θ), electrode-specific reflection phase shifts (ϕ_{bottom}, ϕ_{top}), and resonance orders (m_1, m_2), serving as the mathematical cornerstone for design. Rigorous application of these variables optimizes LOC along the preferred emission direction while simultaneously refining colour purity and angular emission profiles—attributes of paramount importance for high-end display applications, as directly realized in TE configurations.[122]

In TE devices, this optimization manifests through a dense bottom electrode (*e.g.*, Al or Ag), engineered as an opaque, high-reflectivity mirror, paired with a semi-transparent top contact (*e.g.*, ultrathin Ag/ITO/IZO or Ag + MoO_3) functioning as the output coupler. Together, these elements constitute an FP cavity whose optical length is meticulously tuned so that antinodes of the standing electromagnetic wave coincide with the QD recombination zone, extending the interference principles into practical layer engineering. Optimal mirror reflectivities and near-single-mode cavity lengths (m = 1) thereby enables spectral narrowing, Purcell-enhanced spontaneous emission, and effective suppression of waveguide and substrate modes—elevating LOC while highlighting the role of computational validation in sub-micrometre stacks. Contemporary modelling underscores the essential incorporation of MBI effects within CTLs to accurately forecast resonance wavelength and angular emission, bridging theory to fabrication.[123,124]

Achieving the FPR condition thus hinges on multifaceted optimization strategies that build upon this layer-specific tuning, such as incremental adjustments to physical cavity length *via* ITO interlayers and reflection phase engineering of the bottom electrode through metallic structuring. While these modifications deliver clear optical advantages, their influence on stack electronics—such as carrier injection and transport—necessitates comprehensive trade-off analysis at the device level, informing the performance benchmarks that follow.

Performance outcomes from such MC optimization now rival or surpass conventional LOC enhancements in BE analogues, as exemplified by TE-QLEDs featuring modulated mirror penetration depths and low-RI phase-tuning interlayers. These devices attain exceptional peak luminance, EQE, and angular colour stability across wide viewing ranges, all without external scattering elements, demonstrating the framework's capacity for standalone excellence.[108] Hybrid architectures, combining single-mode TE-MC with low-haze scattering caps, further extend this capability to record EQEs with preserved colour invariance, signalling MC's pivotal role in future high-brightness displays.[98] This superior performance is particularly evident in angular emission stability, a defining metric of display quality quantified through chromaticity shifts and luminance uniformity. Single-mode FP-cavity TE-QLEDs exhibit minimal peak wavelength variation and CIE coordinate shifts far below those of multi-cavity or scattering-based alternatives (Fig. 7a and b), outperforming even commercial OLEDs with extended cavities.[27,125] Luminance profiles approximate a moderately Lambertian distribution, affirming the exceptional efficacy of targeted MC tuning in delivering colourimetric and angular emission stability independent of auxiliary architectures (Fig. 7c).[126]

Given colloidal QLEDs' innate ability to produce highly saturated visible emissions, MC engineering plays a central role in overcoming external light extraction limitations, with ongoing innovations amplifying its impact. Techniques such as MC structural refinement, Ag-to-IZO top-electrode substitution to curb angular dispersion, and nanoscale scattering integration collectively enable uniform emission and robust Lambertian profiles—essential traits for next-generation displays (Fig. 8a and b).

Complementing these advances, distributed Bragg reflectors—one-dimensional photonic crystals of alternating high- and low-index layers—offer wavelength-selective reflectivity in TE-QLEDs.[127] This inherent angular dependence, however, requires pairing with redistribution or scattering elements to maintain LOC over broad angles, a consideration reinforced by simulations emphasizing precise optical thickness control above and below the QD layer. Such optimization predicts substantial peak EL intensity gains in TE *versus* BE designs when non-radiative and SPP losses are curtailed (Fig. 8c),[128–132] completing the progression from fundamental interference to holistic device mastery.

4.2 RI tuning

RI tuning mitigates optical losses in QLEDs by reshaping the optical impedance landscape so that excitonic emission preferentially couples into radiative modes rather than waveguide, SPP, or absorptive channels. By moderating index contrast and

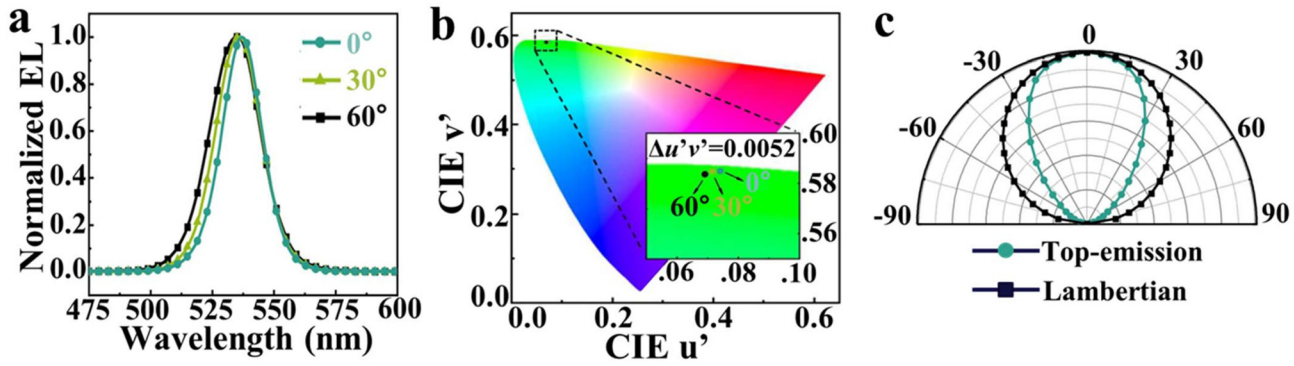

Fig. 7 Angular-dependent emission of TE-QLED device. (a) Nearly invariant EL spectra at different viewing angles. (b) Highly stable CIE 1976 (u′, v′) colour coordinates. (c) Angular luminance pattern close to an ideal Lambertian emitter. ((a)–(c) Reprinted with permission from ref. 108 under a Creative Commons license CC BY 4.0).

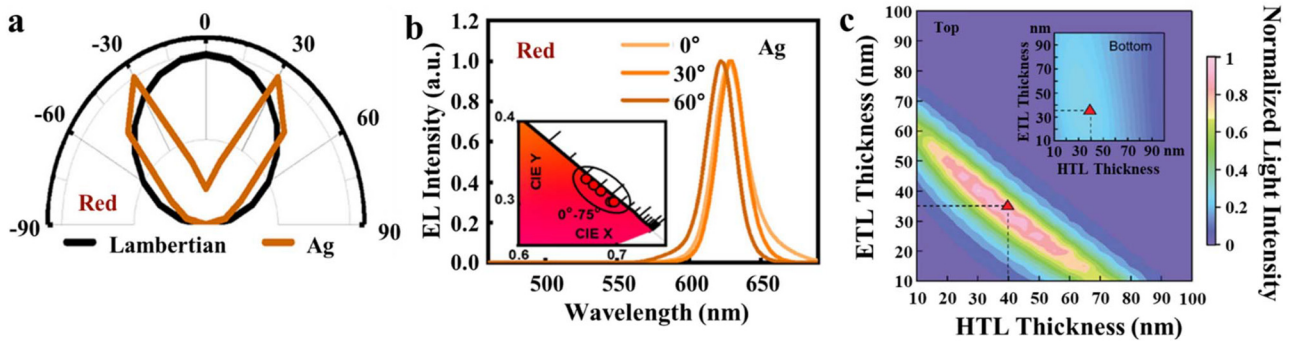

Fig. 8 MC engineering in TE-QLED devices. (a and b) Directional emission and colour shift at wider angles (reprinted with permission from ref. 99. Copyright 2022 American Chemical Society). (c) Optical cavity length adjustment to maximize resonance. (Reprinted with permission from ref. 105. Copyright 2022 John Wiley and Sons).

introducing low-loss dielectric interlayers, it relaxes TIR, displaces standing-wave antinodes away from lossy oxides and metals, and weakens SPP excitation at metal interfaces, thereby redistributing the modal density toward far-field radiation while preserving charge-transport characteristics.

Building on this conceptual basis, the strategic modulation of RI within both the QD EML and adjacent charge-transport materials—particularly ZnMgO nanoparticle layers—has emerged as a critical design lever in TE-QLEDs. By deliberately reducing index contrast at key interfaces, RI tuning simultaneously suppresses waveguide and SPP confinement, driving the angular emission pattern toward a more Lambertian-like distribution and enhancing colour stability across viewing angles. In the representative TE-QLED architecture schematized in Fig. 9a, this optical optimization is integrated into a device layout that otherwise mirrors advanced BE-counterparts, with the crucial addition of a thin ITO interlayer above the Ag mirror to ensure chemical compatibility and robust wetting without sacrificing optical control. Consistent with this philosophy, many reports avoid dielectric top mirrors because their deeper field penetration disrupts single-mode cavity operation, instead favouring ultrathin metal films that combine high reflectance with shallow optical penetration, even though penetration depth definitions are not yet standardized in the literature.[108]

Within this framework, RI tuning at the nanocrystal level provides a practical route to reconciling optical and electronic requirements. As depicted in Fig. 9b, controlled reduction in nanocrystal packing density lowers the effective RI of both the QD (from 1.9 to 1.75) and ZnMgO (from 1.72 to 1.55) layers at the operating wavelength, thereby easing impedance mismatch at internal interfaces. This adjustment enables the assembly of sufficiently thick nanocrystal films to support strong optical interference and field shaping while mitigating undesirable side effects such as increased scattering, field localization near metals, or detrimental changes in transport energetics. In other words, RI tuning here functions as a fine-structure control knob that balances optical mode engineering against carrier mobility and energy-level alignment.

The implications of this balance becomes particularly clear when considering device-level performance metrics. Unlike current efficiency (CE) or operational lifetime, which emphasize forward-direction luminance or stability, EQE captures the total photon flux integrated over all emission directions and thus directly reflects the success of RI-tuned light extraction. In the TE-QLED platform of Fig. 9c and d, combining a shor-

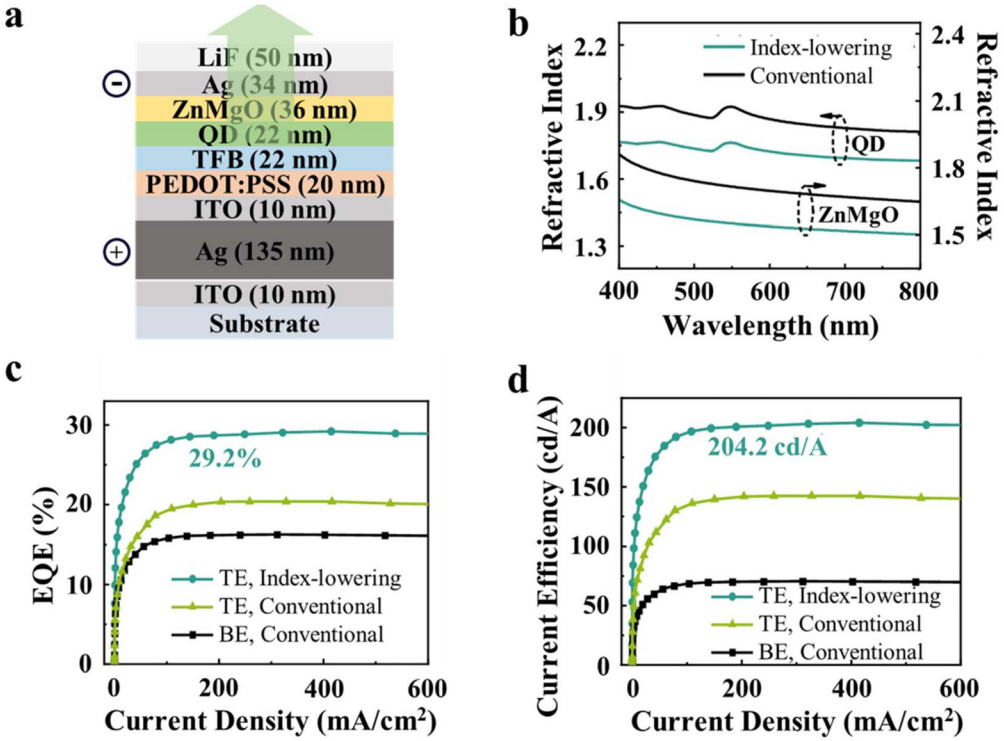

Fig. 9 (a) Illustration of the TE-QLED structure. (b) RI of nanocrystal-assembled films formed using the conventional method and index-lowering process. (c) EQE. (d) CE. The BE device was fabricated using the same semiconductor stacks. The TE device fabricated using the conventional process has a significantly reduced thickness to fit the single-mode resonance. ((a)–(d) Reprinted with permission from ref. 108 under a Creative Commons license CC BY 4.0).

tened optical cavity with a semi-transparent top mirror illustrates how RI optimization can simultaneously elevate total LOC and maintain high forward current efficiency without distorting the emission spectrum. The fact that emission remains centrally weighted near the substrate normal, with negligible penalties at oblique angles, underscores the relevance of RI tuning for display contexts that demand high luminance, low colour distortion, and robust angular performance, such as augmented reality (AR), virtual reality (VR), and high-brightness outdoor applications.

To further generalize these principles beyond QLEDs, Fig. 10a illustrates the conversion of a near-infrared $MAPbI_3$ PeLED into a TE configuration, thereby extending RI-tuning concepts into a chemically distinct material system. In this architecture, a gold bottom anode is selected not only for its optical reflectivity but also for its chemical robustness against halide-induced degradation that typically plagues Ag or Al contacts. A MoO_x interlayer facilitates efficient hole injection, while an ultrathin, Ag-based top electrode—marginally alloyed and deposited under kinetically controlled conditions—achieves high transparency and continuous morphology. The resulting device exhibits strongly forward-directed emission and pronounced angle-dependent spectral shifts, representing a deliberate trade-off away from Lambertian behaviour in favour of highly directional emission, which can be advantageous for certain imaging or projection applications.[133]

Fig. 10b and c then connect these architectural choices to the broader landscape of RI-engineered LOC by mapping the relationship between EQE and both composition and thickness of dielectric LOC layers based on MgF_2, Alq_3, and TeO_2. Each dielectric family exhibits a characteristic optimum thickness where constructive interference and impedance matching coalesce, beyond which interference-driven oscillations in EQE emerge as the optical path deviates from the ideal condition. The appearance of secondary EQE maxima in Alq_3 at larger thicknesses, coupled with their comparable magnitude to the primary peak, highlights the low absorptivity of this organic layer and its suitability for multi-order interference design. The observed non-sinusoidal and asymmetric oscillatory behaviour signals the influence of higher-order optical effects that depend sensitively on device geometry and the electronic landscape, emphasizing that RI tuning must be co-designed with both structural and transport considerations.

The strong agreement between these experimental trends and transfer-matrix method (TMM) simulations provides compelling validation of optical modelling as a predictive tool for RI-engineered outcoupling, including the treatment of self-absorption in perovskite emitters that is mitigated by the use of ultrathin EMLs.[134–136] Within this modelling framework, electrical efficiency—defined as the fraction of injected charges that undergo radiative recombination—emerges as a key fitting parameter that links optical field design to recombination physics.

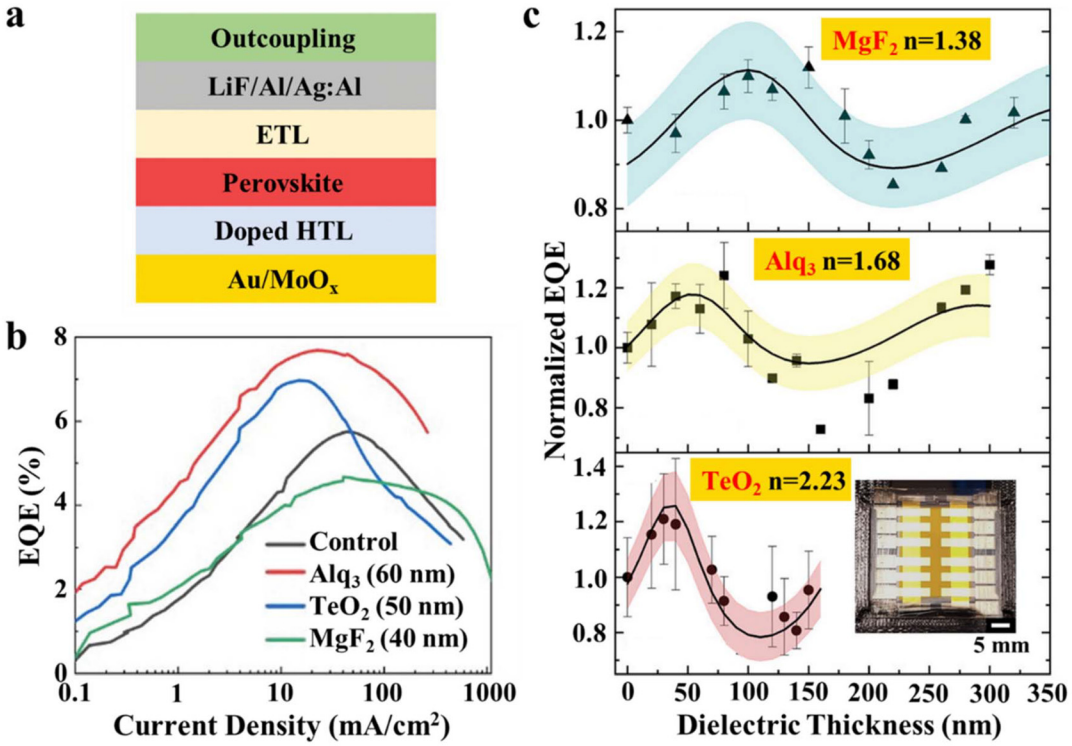

Fig. 10 (a) Schematic diagram of the TE-PeLED architecture. (b) EQE *versus J* for the same devices in (a). (c) Normalized EQE as a function of LOC layer thickness is shown for TE-PeLEDs incorporating (a) MgF_2, (b) Alq_3, or (c) TeO_2 layers. Experimental data points are overlaid with simulation results (solid lines), fitted using the optimal electrical efficiency parameter. The shaded regions represent ±5% variations around this parameter. Inset: photograph of a device sample containing 12 TE pixels defined by the electrode overlap. (Reprinted with permission from ref. 133. Copyright 2024 John Wiley and Sons).

The fact that realistic electrical efficiencies yield close correspondence between calculated and measured EQE confirms that dielectric LOC layers, when combined with RI tuning, provide a genuine physical enhancement rather than an artifact of measurement geometry. Collectively, these results position RI-tuned, dielectric-assisted architectures as a powerful and broadly applicable route to surpassing the optical limitations inherent to conventional BE designs, while retaining compatibility with diverse emissive materials and device platforms.

4.3 Active dipole orientation control

Active dipole orientation control mitigates optical losses in QLEDs by steering excitonic emission into outward-radiating modes rather than dissipative channels, complementing prior MC and RI strategies with emitter-level precision. By engineering QD transition dipoles to favour out-of-plane orientation, the emission pattern couples preferentially to near-normal, extractable modes while minimizing engagement with lateral waveguide modes and SPPs at metal interfaces. This strategic redistribution from lossy, interface-proximal fields enhances light extraction, luminance efficiency, and angular colour stability, establishing a direct bridge to the practical engineering approaches that follow.

Active dipole orientation—specifically horizontal alignment of transition dipole moments parallel to the substrate—has thus emerged as a cornerstone strategy for optimizing LOC across both TE and BE QLED architectures. Horizontal dipoles naturally project photons along the surface normal, aligning with the primary extraction pathway and maximizing EQE, whereas vertical or isotropic orientations favour coupling into trapped waveguide or SPP modes. The critical importance of this control is underscored by the need for precise manipulation through QD shape anisotropy, ligand engineering, and deposition techniques, which collectively minimize optical losses and unlock the full performance potential of QLEDs.

Building on this foundation, investigations into ionicity's role in dipole–dipole interactions have demonstrated how shell composition influences orientation during film formation, as illustrated by polytypic QDs with varied ZnSe/ZnS ratios (Fig. 11a). In solution-processed BE-QLEDs employing an ITO/PEDOT:PSS/TFB/QDs/ZnMgO/Al structure (Fig. 11b), TMM simulations reveal that enhanced in-plane dipole proportions systematically improve theoretical LOC efficiency, with the significance lying in their ability to concentrate emission precisely where extraction geometry demands it.[137] These modelling insights find direct experimental validation in Fig. 11c, where horizontally engineered QLEDs achieve record efficiencies far surpassing isotropic emitters, confirming that anisotropic geometries and mixed crystallographic phases promote favourable inter-dot coupling and planar alignment during assembly.

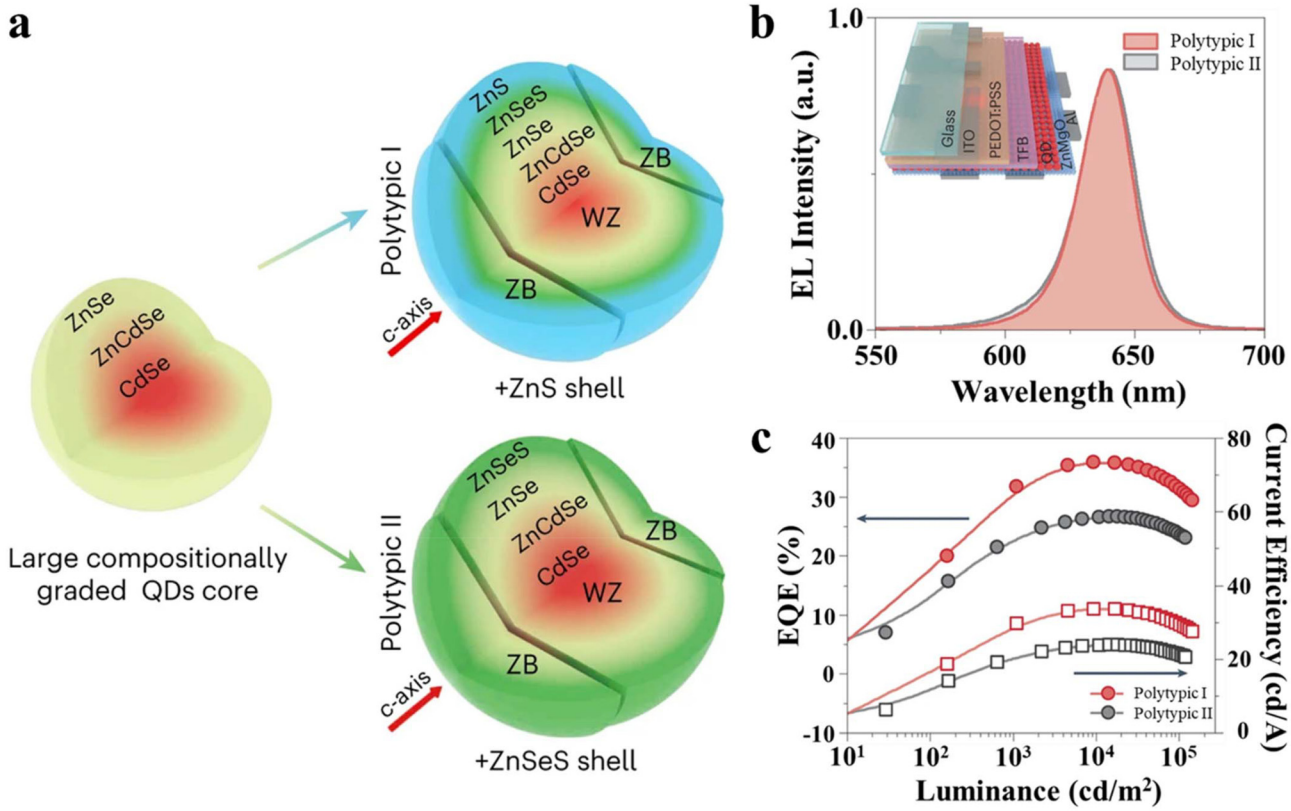

Fig. 11 (a) Synthesis schematic for two types of polytypic QDs with ZnS-rich and -poor outermost shells. (b) EL spectra of polytypic QLEDs with emission peaks at 640 nm. The inset shows a schematic of the QLED architecture. (c) EQEs (solid circles) and CEs (open squares) *versus* luminance. ((a)–(c) Reprinted with permission from ref. 137. Copyright 2024 Springer Nature).

Such alignment, however, demands meticulous control over QD morphology, surface chemistry, and film deposition to overcome random orientations inherent in colloidal synthesis. High-aspect-ratio nanostructures like nanorods or nanoplatelets naturally favour horizontal lying during self-assembly, while tailored ligands and interface treatments reduce orientational disorder and reinforce planar registry. These approaches thus provide a scalable pathway to approach theoretical efficiency limits in TE-QLEDs, setting the stage for advanced assembly techniques that address remaining challenges in isotropic or vertical-dominant systems. In devices retaining isotropic or vertically biased dipoles, substantial light remains confined by TIR or waveguide modes, underscoring the need for next-generation solutions like anisotropic nanocrystal superlattices (ANSLs). Precise assembly of anisotropic QDs—particularly lead halide perovskite nanocrystals—induces preferential horizontal alignment, with the key significance being its ability to preserve single-particle emission directionality into the macroscopic film (Fig. 12).[138] Fig. 12a and b further elucidate how nanocrystal (NC) geometry modulates electric field patterns, with dielectric anisotropy in high-aspect-ratio structures enhancing horizontal dipole output within the critical glass-air escape cone while suppressing vertical emission. Among geometries, square anisotropic NCs prove optimal for LED integration due to substrate compatibility, though maintaining directionality post-assembly requires countering quantum resonance and energy transfer effects observed in materials like edge-on CdSe nanoplatelets. Lead halide perovskite NCs excel here through their high dielectric constants, which effectively screen inter-NC interactions; even ultrathin organic spacers (~0.67 nm) thus suffice to prevent destructive coupling in ANSLs, preserving the engineered emission directionality critical for device performance.

From this fundamental perspective, integrated theory and experiment highlight nanocrystal shape as a pivotal yet historically underexplored determinant of LOC efficiency. Far-field emission pattern calculations across varying anisotropy factors (Fig. 12c) demonstrate self-similar Lambertian profiles whose radiative power increases with shape anisotropy, signifying enhanced device-level LOC without altering angular distribution characteristics. This shape dependence extends to practical device engineering, where HTL selection profoundly influences anisotropic NC assembly in structures like ITO/PEDOT:PSS/HTL/EML/ETL/LiF/Al (Fig. 12d). Since colloidal anisotropic NCs are spin-coated directly onto the HTL, materials like X-F6-TAPC promote superlattice formation more effectively than poly-TPD or HTL-free designs, enabling full angular EL profiling for comprehensive efficiency evaluation. Even modest HTL interlayers enhance current and luminance relative to bare substrates, albeit with subtle efficiency trade-offs that highlight the

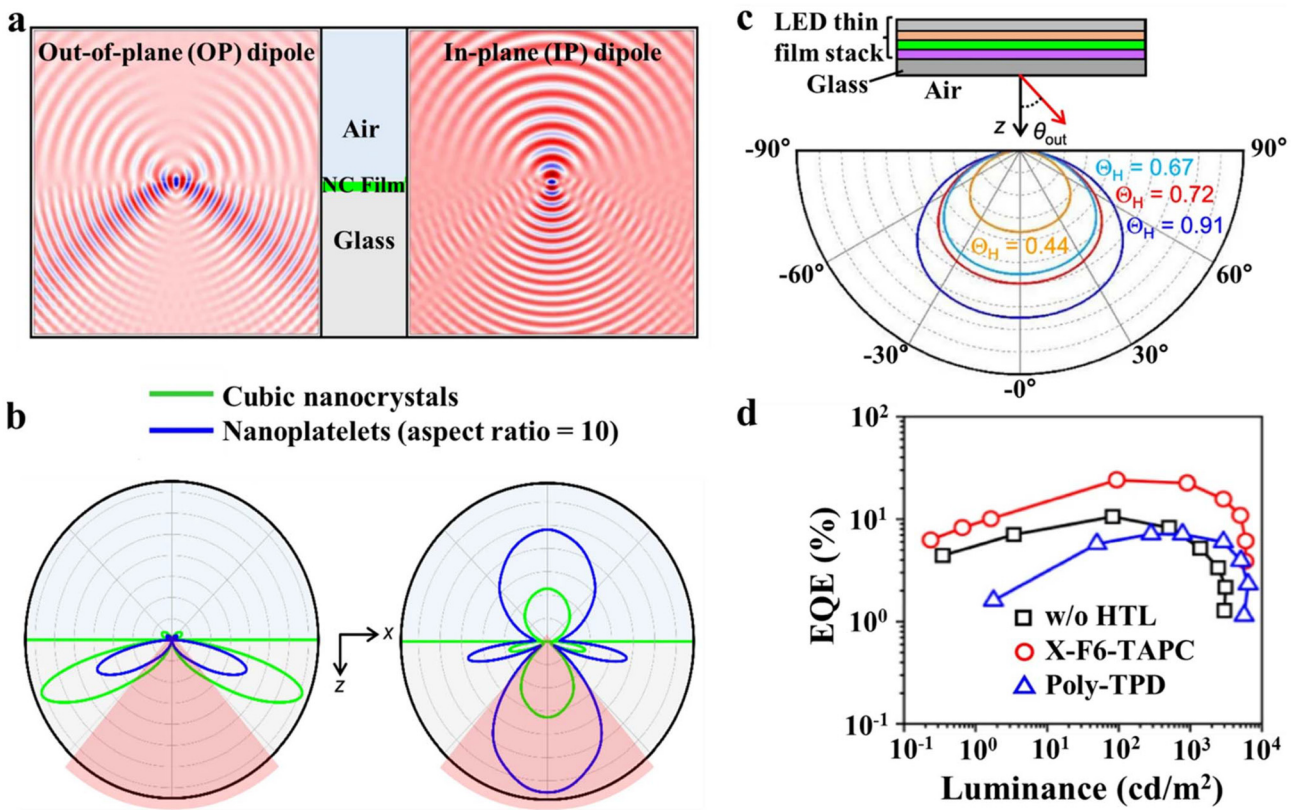

Fig. 12 Polarized emission behaviour in anisotropically dielectric-confined nanocrystals. Calculated electric field intensity profiles (a) and radiation patterns (b) in the *x*–*z* plane are shown for out-of-plane (OP; left) and in-plane (IP; right) dipoles positioned at the centre of a cubic nanocrystal (NC) and an anisotropic nanocrystal (ANC) with an aspect ratio (AR) of 10, embedded in a dielectric emissive film atop a glass substrate. (c) Calculated far-field emission patterns (FEPs) generated by EMLs in optimized LED stack for values of 0.44, 0.67, 0.72, and 0.91, revealing a stronger radiation power outcoupled to air by increasing EML. (d) EQE as a function of luminance for devices incorporating (i) no HTL, (ii) X-F6-TAPC as the HTL, and (iii) poly-TPD as the HTL. (Reprinted with permission from ref. 138 under a Creative Commons license CC BY 4.0).

nuanced interplay between assembly control and charge injection. Ultimately, this work provides the first unified theoretical-experimental validation that high–aspect ratio lead halide perovskite ANSLs faithfully retain individual in-plane dipole orientation, delivering substantial LOC gains in QLEDs. These findings forge a robust, geometry- and assembly-guided framework for QD device design, transforming dipole control from a synthetic challenge into a predictable engineering parameter.

4.4 Surface/interface engineering

Surface and interface engineering mitigates optical losses in QLEDs by tailoring dielectric discontinuities and near-field coupling at critical boundaries, ensuring excitonic emission favours radiative modes over dissipative channels. Carefully selected interlayers and passivation layers increase QD-to–electrode separation and adjust local RIs, thereby weakening SPP excitation, reducing lateral waveguiding at high-contrast interfaces, and suppressing parasitic absorption or destructive interference in defect-rich regions. This boundary-focused approach complements the internal field optimization of prior strategies, establishing the foundation for the escape cone engineering demonstrated below.

The escape cone defines the narrow angular range permitting photon exit from the QD EML into air without TIR, with high-RI QLED layers confining most photons to trapped modes. While RI tuning and MC design expand this escape cone internally, surface engineering directly liberates guided light, as evidenced by the comparison between surface-roughened and conventional QLEDs (Fig. 13a and b). The roughened device's "multi-pit" morphology reduces glass/air reflection and suppresses waveguide confinement, enabling multiple escape pathways (top escape cone, top plane, and side planes) rather than the conventional device's edge-dominated emission. Visible substrate illumination in planar devices confirms bottom–interface losses, while ray-tracing validates scattering, refraction, and absorption dynamics across all surfaces.[139]

This principle finds practical embodiment in surface-roughened QLEDs fabricated by etching the glass/air interface within a glass/ITO/PEDOT:PSS/poly-TPD/CdSe-CdS-ZnS QD/ZnO/Al stack (Fig. 13c). Roughening dramatically enhances extraction, with benefits compounding at higher voltages due to increased internal generation (Fig. 13d). The resulting EQE improvement and delayed roll-off signify reduced voltage sensitivity, while brightness gains reflect enhanced photon through-

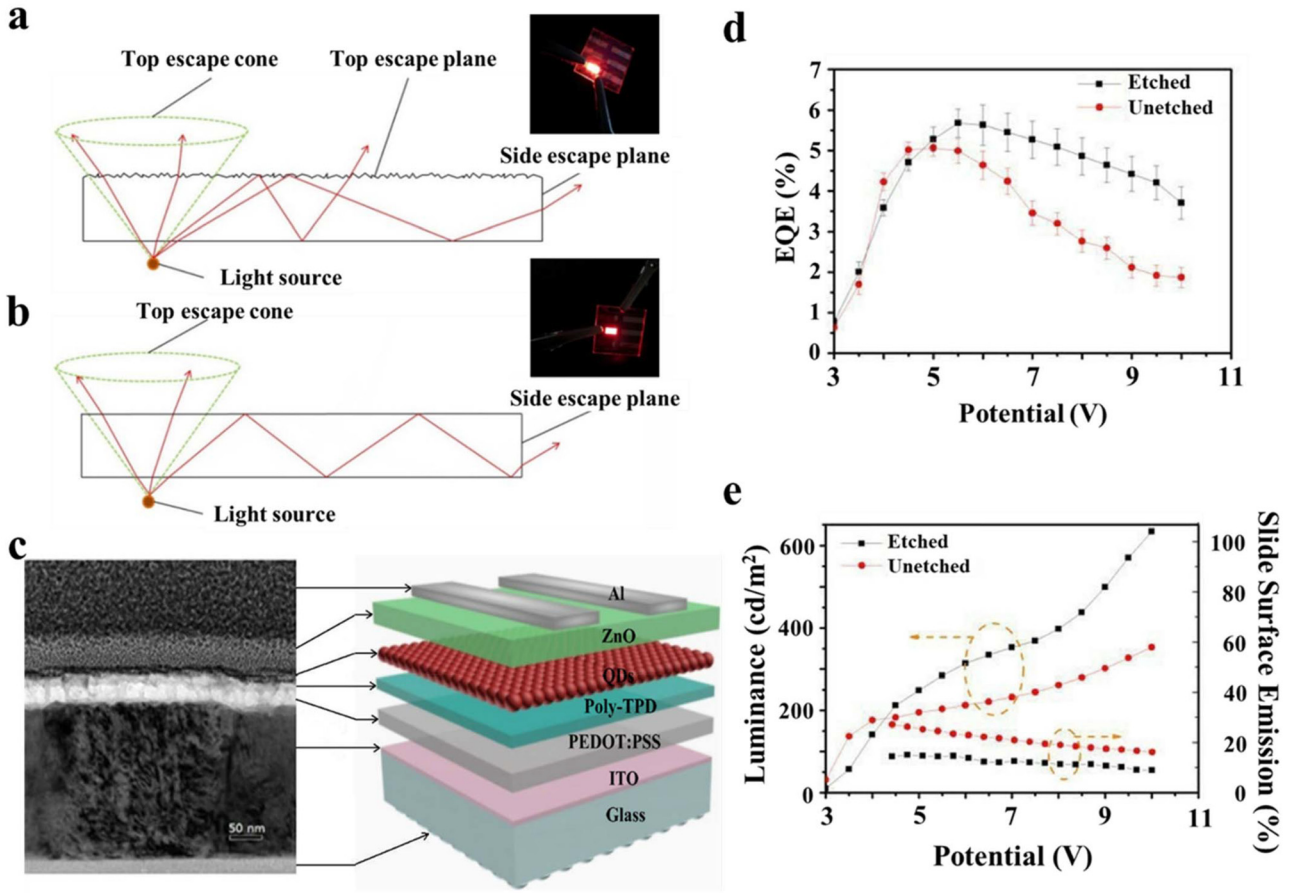

Fig. 13 The relation between QLED performance and optical/electrical parameters. The light has (a) three escape modes for surface roughened QLED and (b) two escape modes for conventional QLED in glass substrate. (c) Cross-sectional transmission electron microscopy image and schematic device structure of surface roughened QLEDs. (d) The EQE-voltage characteristics. (e) The luminance–voltage characteristics. ((a)–(e) Reprinted with permission from ref. 139. Copyright 2017 Optical Society of America).

put (Fig. 13e). Critically, diminished side emission confirms redirection toward the TE surface, aligning seamlessly with theoretical predictions and paving the way for advanced nanosphere-based scattering.

4.4.1 Nanosphere surface. Nanosphere layers atop TE-QLEDs extend surface roughening principles through controlled curvature and RI variation, disrupting TIR to liberate internally confined modes. As scattering centres, nanospheres redirect waveguided light into the escape cone while recovering absorption-bound photons, simultaneously broadening angular emission for improved uniformity without viewing-angle colour dependence. This forward-directed enhancement elevates current efficiency and display performance, naturally transitioning to the specific TE-QLED architecture of Fig. 14a. In this structure, a reflective Ag bottom anode pairs with transparent IZO top cathode, while an ultrathin Al-buffered ZnMgO ETL shields the QD EML from sputtering damage. TE geometry eliminates substrate waveguide modes and reduces absorption/SPP losses, yet high layer/air RI contrast sustains TIR confinement (Fig. 14b). Nanosphere integration breaks this limitation, as confirmed by PL measurements on glass/QD/ZnMgO/Al/IZO test structures. Optimizing MC effects through ZnMgO thickness tuning yields champion red TE-QLEDs demonstrating record performance with exceptional batch reproducibility across colours, underscoring the approach's robustness (Fig. 14c).

For displays, where current efficiency quantifies forward emission, angularly resolved measurements (Fig. 14d inset), enable precise efficiency derivation. Nanosphere incorporation substantially improves this metric by expanding the emission solid angle, confirming purely optical enhancement that builds toward more sophisticated nano-scattering implementations.

4.4.2 Nano-scattering layer. Nano-scattering layers atop TE-QLED top electrodes advance beyond nanosphere scattering by addressing MC-imposed LOC constraints through localized RI modulation. This strategic TIR disruption converts waveguide and SPP modes into escape-cone radiative channels, mitigating the non-radiative losses responsible for internal photon trapping while extending angular coverage for enhanced luminance uniformity.

In benchmark inverted TE-QLEDs featuring Ag cathode, ZnO nanoparticle ETL, multi-shell [ZnSeTe/ZnSe/ZnS] QD EML, organic HTLs (CzSi/TCTA), MoO_x hole injection layer (HIL), and thin Ag anode (Fig. 15a), structured capping planarization layers (SCPLs) with controlled nanoscale morphology

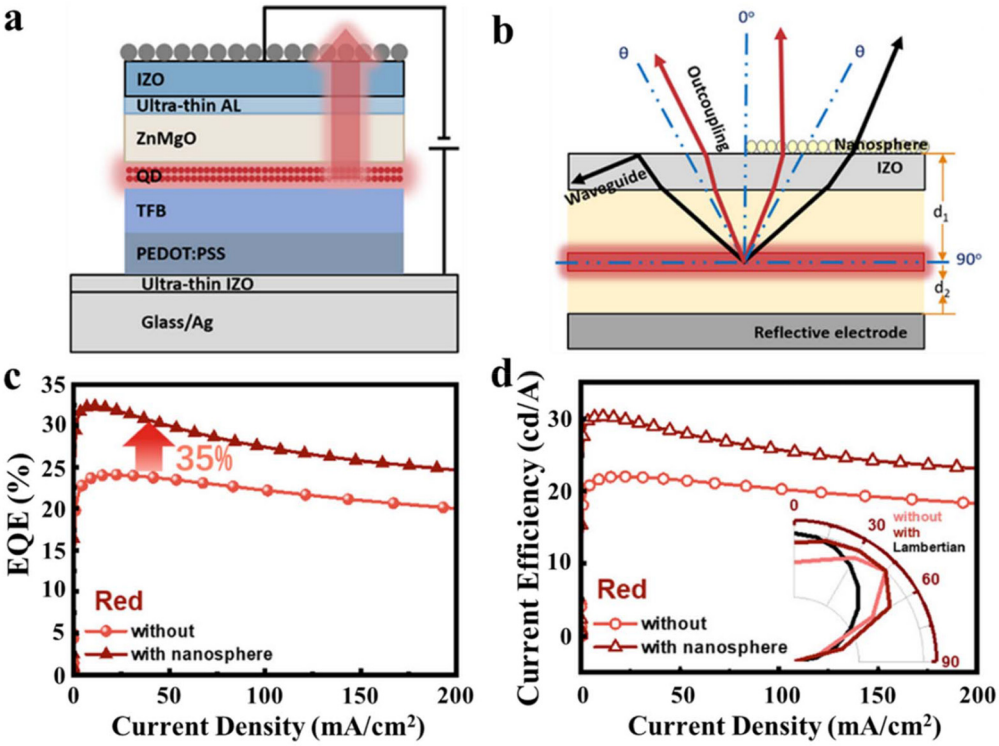

Fig. 14 TE-QLEDs with the IZO top electrode and SiO_2 nanosphere scattering layer. (a) Device structure. (b) Schematic illustration of the LOC principle. With the nanospheres, the black arrow which refers to the originally waveguided light can be coupled out to air. The EQE–*J* curves of (c) red TE-QLEDs with or without nanospheres. The CE–*J* curves of (d) red TE-QLEDs with or without nanospheres. The insets show the corresponding angular emission pattern of devices. ((a)–(d) Reprinted with permission from ref. 104. Copyright 2022 American Chemical Society).

outperform conventional planar layers.[140] The enhancement arises predominantly from improved LOC rather than IQE, confirming the optical origin (Fig. 15b).

Scattering efficacy peaks at optimal nano-crack density within SCPLs, where sub-wavelength ZnO agglomerates and distributed cracks create a heterogeneous landscape fostering multiple scattering events that recouple trapped modes (Fig. 15c). Mechanistically, thickness-dependent interference redistributes EL spectrally and angularly, while nanoscale heterogeneity amplifies scattering cross-sections and photon randomization, culminating in momentum relaxation and superior extraction. This versatility extends to TiO_2, SiO_2, and NiO alternatives, broadening materials compatibility.

4.4.3 Microlens array. Microlens arrays (MLAs) mitigate TIR, Fresnel reflections, and substrate-guided losses through geometric optical modulation of the device–air boundary. By locally reshaping surface normals, MLAs broaden the escape cone and redirect emission beyond the critical angle, unlocking photons otherwise confined within waveguide or substrate modes. Functioning effectively as adiabatic RI gradients, they reduce reflection losses across wide angular ranges, particularly at high incidence angles where Fresnel reflection is most pronounced. This controlled redirection enhances forward luminance and far-field angular uniformity—key for maintaining consistent brightness and colour fidelity in high-resolution display applications.

However, purely geometric optics approaches cannot fully address deeply guided or cavity-confined modes. The ray-optical framework of an MLA inherently limits its coupling strength to high-order waveguide modes or SPP resonances, which constitute significant reservoirs of trapped energy in thin-film EL architectures. This limitation naturally motivates hybrid strategies that integrate subwavelength scattering mechanisms to complement the macroscopic optical shaping provided by MLAs, creating multi-scale light extraction channels spanning both geometric and diffractive regimes.

Embedding Mie-resonant dielectric nanospheres (for example, SiO_2, ~600 nm in diameter) within or atop MLAs introduces wave-optical synergy that bridges these regimes. The nanosphere ensemble produces broadband and angle-insensitive scattering capable of coupling guided and evanescent modes into free-space radiation. This hybrid structure enhances LOC efficiency without spectral distortion, yielding quasi-Lambertian emission and superior angular uniformity (Fig. 16a–c). Additionally, the redistribution of optical power reduces photon recycling and Joule heating, improving device stability and operational lifetime.[141–143] While MLAs alone can significantly boost EQE, coupling them with resonant dielectric scatterers achieves simultaneous gains in extraction, luminance, and angular balance, offering a scalable pathway toward optically optimized and high-definition QLED displays.[144,145]

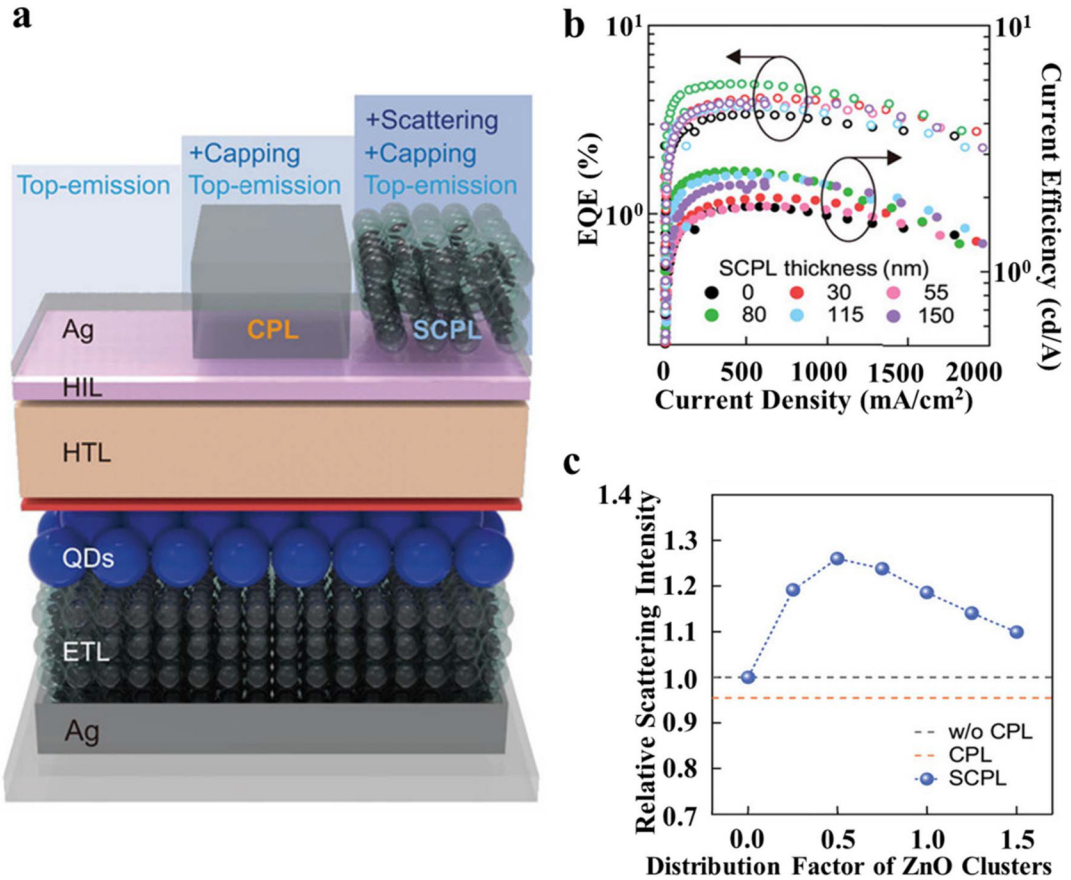

Fig. 15 (a) Schematic illustration of the TE ZnSeTe/ZnSe/ZnS QLEDs without a CPL, with the conventional CPL and the SCPL. (b) The EQE and CE of the QLEDs with the SCPL thicknesses of 0, 30, 55, 80, 115, or 150 nm. (c) Relative scattering intensity of the QLEDs with the 80 nm-thick SCPL to the device without a CPL, as a function of ρ. Error bars are the standard deviations of the results from 20 realizations. The dashed lines are the scattering intensities of QLEDs without a CPL (gray) and with the conventional CPL (90 nm, orange). ((a)–(c) Reprinted with permission from ref. 140. Copyright 2024 John Wiley and Sons).

4.4.4 Wrinkled surface/interface. Wrinkled surfaces transform planar QLEDs into omnidirectional emitters through broadband, nonresonant scattering that shatters TIR confinement (Fig. 17a and b).[146–148] Unlike periodic gratings introducing colour shifts, quasi-aperiodic wrinkles generate dense reciprocal-lattice vectors coupling all azimuthal guided modes into the escape cone without spectral distortion, converting waveguide, SPP, and interference losses into useful emission while approaching Lambertianity. While focusing on patterning, disorder suppression can be achieved through capillary forces that minimize structural imperfections and reduce nonradiative recombination—contrasting sharply with the inherently stochastic nature of conventional wrinkle formation.[149] Quasi-aperiodic wrinkles excel in broadband, omnidirectional scattering across all azimuthal modes without inducing colour shifts. However, introducing controlled long-range order could hybridize their optical behaviour. Ordered wrinkle arrays, achieved through capillary-templated buckling, would preserve the wide-period and random-directionality benefits of wrinkles while mitigating defect-induced quenching, potentially enabling >30% EQE enhancement in high-PPI blue QLEDs without optical crosstalk. This approach merges the scattering isotropy of wrinkling with the electrical stability of deterministic surface patterning.

EQE-luminance characteristics verify that the improvement arises purely from optical effects across operating range, with preserved roll-off behaviour indicating unaffected recombination dynamics (Fig. 17c). The high, wavelength-independent spectral haze further corroborates broadband forward scattering driven by RI modulation. Formed through mechanical instabilities in polymeric overlayers, wrinkles provide a scalable and cost-effective route for large-area implementation, positioning them as a versatile platform for surface-engineered light extraction.

This top-surface philosophy extends naturally to buried CTL interfaces. Controlled ZnO ETL roughening on ITO—achieved *via* deposition-rate modulation—creates internal Mie-scattering centres at the ZnO/QD boundary (Fig. 18a inset). Moderate surface roughness strengthens CE by enabling balanced charge injection and guided-mode LOC (Fig. 18b), while spectrally smooth haze spectra confirm their role as buried optical extractors (Fig. 18c). Optimization requires carefully balancing

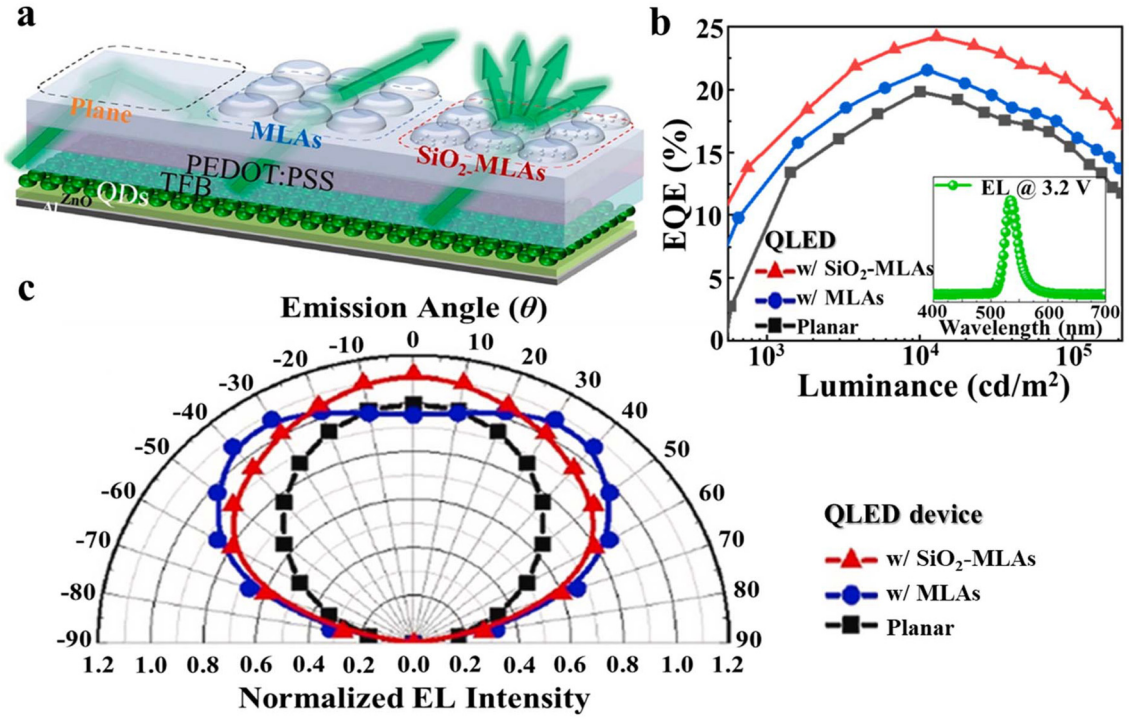

Fig. 16 (a) SiO_2-MLA composite structures fabricated by the imprint on SiO_2-nanosphere thin film. (b) EQE-luminance performance of green-QLED with SiO_2-MLAs and reference structure. (c) The relationship between QLED luminous intensity and exit angle at 5 V. ((a)–(c) Reprinted with permission from ref. 144. Copyright 2025 Elsevier).

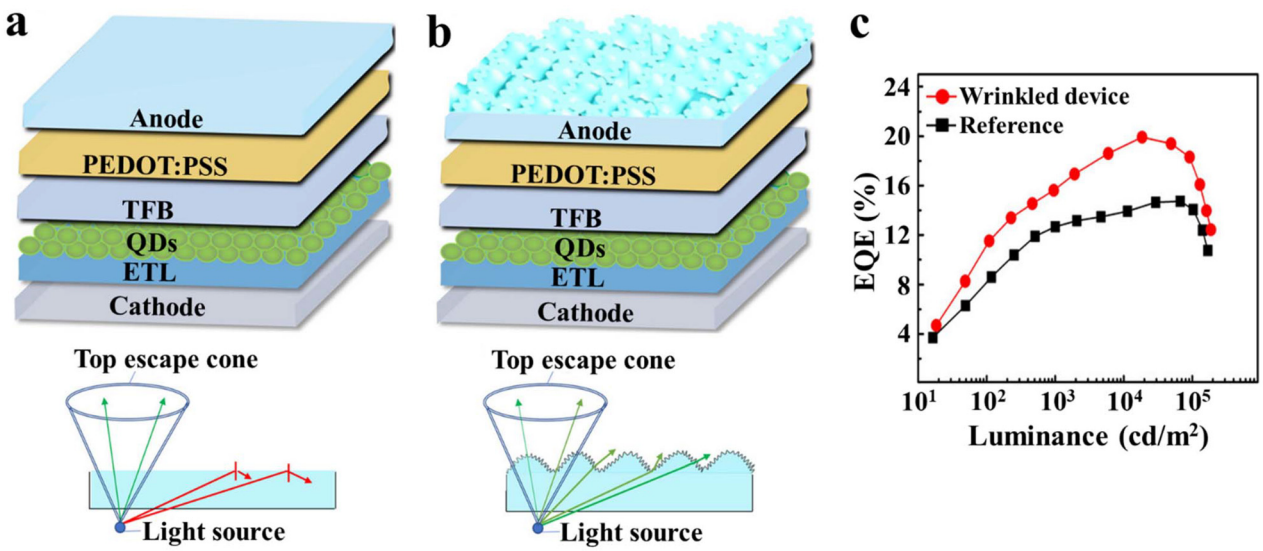

Fig. 17 Wrinkled light-extraction structure of QLEDs. (a) Schematic of the planar QLED showing limited LOC by TIR within the top escape cone. (b) Schematic of the wrinkled anode structure that scatters waveguide modes into the escape cone to enhance light extraction. (c) EQE as a function of luminance for the wrinkled and reference QLEDs, showing improved efficiency with the wrinkled structure. (Reprinted with permission from ref. 146. Copyright 2025 John Wiley and Sons).

optical gains with recombination stability, achieving simultaneous three-dimensional and multi-interface control.

Micro- and nanostructured geometries such as pyramids, cylinders, and moth-eye textures further expand this design toolkit by introducing graded RI profiles and directional scattering. These architectures enhance EQE, luminance, and thermal stability,[150–153] while geometric optimization of features such as period, height, and duty cycle prevents mechanical or electrical degradation. Although interfacial texturing enhances light extraction, it also introduces challenges such as field pertur-

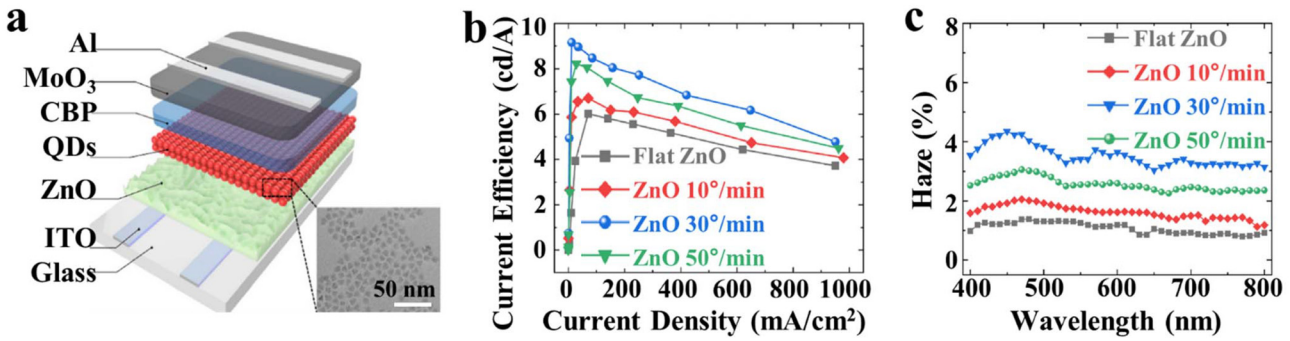

Fig. 18 Interface wrinkling in ZnO ETLs for buried LOC. (a) Schematic of ITO/ZnO/QD/CBP/MoO_3/Al QLED with varying ZnO growth rates inducing interfacial roughness (TEM inset). (b) Current efficiency *vs.* density showing optimal enhancement at moderate roughening. (c) Spectral haze confirming broadband scattering from nanostructured interfaces. (Reprinted with permission from ref. 147. Copyright 2020 Optical Society of America).

bation, instability, and roughness-induced degradation. Reliable implementation therefore demands robust materials, ultrathin passivation, precision ALD, and compliant interlayers.

4.5 Synergistic interactions and integration challenges

Integrating MC engineering, RI modulation, dipole orientation control, and surface/interface engineering transcends individual limitations but demands careful reconciliation of competing constraints.[33,137,151,154,155] MC layer thickness and RI requirements for constructive interference must harmonize with charge transport distances and dipole alignment preferences, ensuring optical precision reinforces electrical balance.

Horizontal dipole engineering maximizes forward extraction in thin cavities, yet aggressive surface nanopatterning risks disrupting alignment or local fields, requiring process harmonization. RI modulation broadens the extraction cone while nanostructures scatter residual modes, but excessive texturing invites absorption or injection damage, necessitating co-optimization of dimensions with functional stack properties.

Combined strategies yield nonlinear gains due to overlapping mechanisms and emergent losses—cavity thickening, metallic reflectance, or carrier imbalance capping ultimate efficiency. True synergy emerges through spectrum-specific, angular-tailored tuning that respects layer conductivity, transforming potential conflicts into coherent, device-level mastery.

5. Conclusions and future outlook

Optimizing LOC remains among the most persistent and intellectually intricate challenges in advancing TE-QLEDs. In this review, four unifying strategies have been delineated: MC resonance engineering, RI modulation, active dipole orientation control, and surface/interface engineering, each addressing distinct facets of photon confinement and loss. Collectively, these schemes mitigate optical dissipation by suppressing waveguide, SPP, and absorption/interference modes, thereby enabling TE-QLEDs with refined emission directionality, elevated EQE, and enhanced colour purity. Together, they form an integrated conceptual and experimental framework for achieving precise optical confinement, balanced charge transport, and high-fidelity luminescence in next-generation display architectures.

Looking forward, the intersection of materials science, optical physics, and computational design signals a paradigm shift in the control of light–matter interactions at the nanoscale. The infusion of machine learning and artificial intelligence into LOC optimization represents a transformative evolution in photonic device engineering. Through inverse design algorithms, evolutionary optimization, and deep generative modelling, complex optical design landscapes can now be explored with unprecedented efficiency. These approaches promise automated discovery of metastructures exhibiting tailored emission profiles, angular uniformity, and fabrication tolerance, outperforming the heuristic limitations of manual parametric tuning. In this emerging data-driven framework, the feedback loop among simulation, prediction, and fabrication becomes increasingly self-optimizing, thereby fostering rapid convergence toward devices that operate near the theoretical limits of optical performance.

In parallel, scalability and manufacturability will determine the translational viability of advanced LOC strategies. Achieving high-fidelity nanophotonic patterning across large, flexible, and transparent substrates remains a formidable engineering frontier. Promising developments in nanoimprint lithography, block copolymer self-assembly, and ALD-assisted nanostructure growth are opening viable routes toward wafer-scale realization of subwavelength optical architectures with atomic precision. However, harmonizing these sophisticated fabrication schemes with industrial productivity, cost efficiency, and mechanical robustness remains critical for the practical integration of QLED technologies into commercial display applications.

Beyond fabrication, the implementation of advanced LOC designs must also address complex trade-offs among optical efficiency, angular stability, and operational longevity. High-order resonant structures, although capable of significant enhancements in directionality and spectral purity, are inherently susceptible to angular dispersion and resonant heating.

The development of robust optical architectures that preserve spectral invariance across wide viewing angles, while suppressing exciton–plasmon quenching and photothermal degradation, will be essential to achieving stable and colour-pure emission. Such stability requires holistic co-optimization of optical confinement, thermal management, and excitonic dynamics within a single device platform.

Equally important is the deliberate control of interfacial quantum coupling, which governs charge balance, exciton recombination dynamics, and device stability. By adjusting interfacial dipole distributions, barrier asymmetry, and molecular alignment at the QD–CTL junction, it becomes possible to fine-tune radiative and nonradiative recombination pathways. Coupling this interfacial design with advanced characterization techniques such as time-resolved photoluminescence, *in situ* spectroelectronics, and ultrafast transient spectroscopy will be essential for establishing direct correlations between microscopic interfacial structure and macroscopic optoelectronic behaviour.

Finally, the integration of gradient-index photonics with deterministic dipole alignment offers a promising route toward ultimate light extraction and emission control. Hybrid architectures composed of multilayer dielectric nanolaminates, tuneable metal–insulator–metal (MIM) cavities, and anisotropic organic matrices can sculpt photon flow within the optical MC, enabling near-lossless light extraction and precise spectral modulation. When combined with nanoscale control over QD morphology, ligand chemistry, and local electromagnetic field coupling, such designs could elevate TE-QLEDs to performance regimes approaching the theoretical radiative limits of nanocrystal emitters, with enhanced stability and diffraction-limited angular precision.

Author contributions

All authors discussed and wrote the manuscript together. All authors read and approved the final manuscript.

Conflicts of interest

There are no conflicts to declare.

Abbreviations

ALD	Atomic layer deposition
ANSLs	Anisotropic nanocrystal superlattices
BE-QLEDs	Bottom-emitting QLEDs
CdSe	Cadmium selenide
CPL	Charge transport and planarization layer
cQDs	Colloidal quantum dots
CTLs	Charge transport layers
EIL	Electron injection layer
EL	Electroluminescence
EML	Emission material layer
EQE	External quantum efficiency
ETL	Electron transport layer
FEPs	Far-field emission patterns
FWHM	Full-width at half maximum
FPR	Fabry-Pérot resonance
HAT-CN	1,4,5,8,9,11-Hexaazatriphenylene hexacarbonitrile
HIL	Hole injection layer
HOMO	Highest occupied molecular orbital
HTL	Hole transport layer
InP	Indium phosphide
IQE	Internal quantum efficiency
ITO	Indium tin oxide
LEDs	Light emitting diodes
LEE	Light extraction efficiency
LHP	Lead halide perovskite
LUMO	Lowest unoccupied molecular orbital
MBI	Multiple-beam interference
MC	Microcavity
MLA	Microlens array
MoO_3	Molybdenum trioxide
LOC	Light outcoupling
OLEDs	Organic LEDs
PEDOT:PSS	Poly-3,4-ethylendioxythiophen:polystyrene sulfonate
PeLEDs	Perovskite LEDs
PL	Photoluminescence
PLQY	Photoluminescence quantum yield
QDs	Quantum dots
QLEDs	Quantum dot LEDs
RI	Refractive index
SCPL	Structured CPL
SPP	Surface plasmon polariton
TCTA	Tris(4-carbazoyl-9-ylphenyl)amine
TFB	Poly(9,9-dioctylfluorene-*alt*-*N*-(4-sec-butylphenyl)-diphenylamine)
TE-QLEDs	Top-emitting QLEDs
TIR	Total internal reflection
TMM	Transfer-matrix method
TPBi	1,3,5-Tris(1-phenyl-1*H*-benzimidazol-2-yl)benzene
ZnSeTe	Zinc selenide telluride

Data availability

No primary research results, software or code have been included and no new data were generated or analysed as part of this review.

Acknowledgements

This work was supported by the National Research Foundation of Korea grant funded by the Korea government (MSIT) (RS-2024-00411892, RS-2025-23323726 and RS-2025-02217649) and Korea Institute for Advancement of Technology (KIAT) grant funded by the Korean Government (MOTIE) (RS-2025-02263458, HRD

Program for Industrial Innovation). This work was also supported from the Korea Basic Science Institute (National Research Facilities and Equipment Center) grant funded by the Ministry of Education (grant no. 2021R1A6C101A405).

References

1 Z.-K. Tan, R. S. Moghaddam, M. L. Lai, P. Docampo, R. Higler, F. Deschler, M. Price, A. Sadhanala, L. M. Pazos, D. Credgington, F. Hanusch, T. Bein, H. J. Snaith and R. H. Friend, *Nat. Nanotechnol.*, 2014, **9**, 687, DOI: 10.1038/nnano.2014.149.

2 M. Lu, J. Guo, S. Sun, P. Lu, X. Zhang, Z. Shi, W. W. Yu and Y. Zhang, *Chem. Eng. J.*, 2021, **404**, 126563, DOI: 10.1016/j.cej.2020.126563.

3 Y. Lou, M. Fang, J. Chen and Y. Zhao, *Chem. Commun.*, 2018, **54**, 3779, DOI: 10.1039/C8CC01110A.

4 O. Voznyy, L. Levina, J. Z. Fan, M. Askerka, A. Jain, M.-J. Choi, O. Ouellette, P. Todorovic, L. K. Sagar and E. H. Sargent, *ACS Nano*, 2019, **13**, 11122, DOI: 10.1021/acsnano.9b03864.

5 O. Chen, J. Zhao, V. P. Chauhan, J. Cui, C. Wong, D. K. Harris, H. Wei, H.-S. Han, D. Fukumura, R. K. Jain and M. G. Bawendi, *Nat. Mater.*, 2013, **12**, 445, DOI: 10.1038/nmat3539.

6 Z. Chen, X. Chen, Y. Xiao, S. Ren and Y. Li, *Adv. Sci.*, 2025, e05737, DOI: 10.1002/advs.202505737.

7 S. Coe, W. K. Woo, M. Bawendi and V. Bulovic, *Nature*, 2002, **420**, 800, DOI: 10.1038/nature01217.

8 Y. H. Won, O. Cho, T. Kim, D. Y. Chung, T. Kim, H. Chung, H. Jang, J. Lee, D. Kim and E. Jang, *Nature*, 2019, **575**, 634, DOI: 10.1038/s41586-019-1771-5.

9 Y. Deng, F. Peng and Y. Lu, *Nat. Photonics*, 2022, **16**, 505, DOI: 10.1038/s41566-022-00999-9.

10 P. Yu, S. Cao, Y. Shan, Y. Bi, Y. Hu, R. Zeng, B. Zou, Y. Wang and J. Zhao, *Light: Sci. Appl.*, 2022, **11**, 162, DOI: 10.1038/s41377-022-00855-z.

11 P. Yu, Y. Shan, S. Cao, Y. Hu, Q. Li, R. Zeng, B. Zou, Y. Wang and J. Zhao, *ACS Energy Lett.*, 2021, **6**, 2697, DOI: 10.1021/acsenergylett.1c01067.

12 Q. Li, S. Cao, P. Yu, M. Ning, K. Xing, Z. Du, B. Zou and J. Zhao, *Photonics Res.*, 2022, **10**, 2133, DOI: 10.1364/prj.467604.

13 W.-C. Chao, T.-H. Chiang, Y.-C. Liu, Z.-X. Huang, C.-C. Liao, C.-H. Chu, C.-H. Wang, H.-W. Tseng, W.-Y. Hung and P.-T. Chou, *Commun. Mater.*, 2021, **2**, 96, DOI: 10.1038/s43246-021-00203-5.

14 H. Li, Y. Bian, W. Zhang, Z. Wu, T. K. Ahn, H. Shen and Z. Du, *Adv. Funct. Mater.*, 2022, **32**, 2204529, DOI: 10.1002/adfm.202204529.

15 H. Li, W. Zhang, Y. Bian, T. K. Ahn, H. Shen and B. Ji, *Nano Lett.*, 2022, **22**, 4067, DOI: 10.1021/acs.nanolett.2c00763.

16 N. N. Mude, S. J. Kim, R. Lampande and J. H. Kwon, *Nanoscale Adv.*, 2022, **4**, 904, DOI: 10.1039/d1na00716e.

17 P. Liu, Y. Lou, S. Ding, W. Zhang, Z. Wu, H. Yang, B. Xu, K. Wang and X. W. Sun, *Adv. Funct. Mater.*, 2021, **31**, 2008453, DOI: 10.1002/adfm.202008453.

18 K. D. Nolf, R. C. Capek, S. Abe, M. Sluydts, Y. Jang, J. C. Martins, S. Cottenier, E. Lifshitz and Z. Hens, *J. Am. Chem. Soc.*, 2015, **137**, 2495, DOI: 10.1021/ja509941g.

19 S. Lyssenko, M. Amar, A. Sermiagin, A. Barbora and R. Minnes, *Sci. Rep.*, 2025, **15**, 2630, DOI: 10.1038/s41598-025-86026-7.

20 J. Park, A. Jayaraman, A. W. Schrader, G. W. Hwang and H.-S. Han, *Nat. Commun.*, 2020, **11**, 5748, DOI: 10.1038/s41467-020-19573-4.

21 G. Zaiats, S. Ikeda, S. Kinge and P. V. Kamat, *ACS Appl. Mater. Interfaces*, 2017, **9**, 30741, DOI: 10.1021/acsami.7b07893.

22 K. H. Lee, J. H. Lee, H. D. Kang, B. Park, Y. Kwon, H. Ko, C. Lee, J. Lee and H. Yang, *ACS Nano*, 2014, **8**, 4893, DOI: 10.1021/nn500852g.

23 K. H. Lee, J. H. Lee, W. S. Song, H. Ko, C. Lee, J. H. Lee and H. Yang, *ACS Nano*, 2013, **7**, 7295, DOI: 10.1021/nn402870e.

24 X. Yang, E. Mutlugun, C. Dang, K. Dev, Y. Gao, S. T. Tan, X. W. Sun and H. V. Demir, *ACS Nano*, 2014, **8**, 8224, DOI: 10.1021/nn502588k.

25 C. Jeong, Y.-B. Park and L. J. Guo, *Sci. Adv.*, 2021, **7**, eabg0355, DOI: 10.1126/sciadv.abg0355.

26 Y. Zhang, W. Wang, F. Zheng, J. Jhu, G. Mei, Y. Ye, J. Tan, H. Zhang, Q. Jing, B. He, K. Wang and D. Wu, *Photonics*, 2025, **12**, 427, DOI: 10.3390/photonics12050427.

27 H. Li, J. Wang and S. Chen, *Light: Sci. Appl.*, 2025, **14**, 171, DOI: 10.1038/s41377-025-01835-9.

28 Z. Liu, F. Li, G. Huang, J. Wei, G. Jiang and Y. Huang, *J. Nanomater.*, 2020, **9**, 1, DOI: 10.1155/2020/8858996.

29 S. Park, B. Kang, S. Lee, J. C. Bi, J. Park, Y. H. Hwang, J.-Y. Park, H. Hwang, Y. W. Park and B.-K. Ju, *Micromachines*, 2024, **15**, 328, DOI: 10.3390/mi15030328.

30 O. Hill, M. Wollweber, T. Biermann, T. Ripken and R. Lachmayer, *J. Biomed. Opt.*, 2024, **29**, 066004, DOI: 10.1117/1.JBO.29.6.066004.

31 Y. Guo, M. C. Weidman and W. A. Tisdale, *Nano Lett.*, 2017, **17**, 3837, DOI: 10.1021/acs.nanolett.7b01237.

32 M. J. Jurow, T. Morgenstern, C. Eisler, J. Kang, E. Penzo, M. Do, M. Engelmayer, W. T. Osowiecki, Y. Bekenstein, C. Tassone, L.-W. Wang, A. P. Alivisatos, W. Brutting and Y. Liu, *Nano Lett.*, 2019, **19**, 2489, DOI: 10.1021/acs.nanolett.9b00122.

33 Q. Wan, W. Zheng, C. Zou, F. Carulli, C. Zhang, H. Song, M. Liu, Q. Zhang, L. Y. Lin, L. Kong, L. Li and S. Brovelli, *ACS Energy Lett.*, 2023, **8**, 927, DOI: 10.1021/acsenergylett.2c02802.

34 J. Ye, A. Ren, L. Dai, T. K. Baikie, R. Guo, D. Pal, S. Gorgon, J. E. Heger, J. Huang, Y. Sun, R. Arul, G. Grimaldi, K. Zhang, J. Shamsi, Y.-T. Huang, H. Wang, J. Wu, A. F. Koenderink, L. T. Murciano, M. Schwartzkopf, S. V. Roth, P. Muller-Buschbaum, J. L. Baumberg, S. D. Stranks, N. C. Greenham, L. Polavarapu, W. Zhang,

A. Rao and R. L. Z. Hoye, *Nat. Photonics*, 2024, **16**, 586, DOI: 10.1038/s41566-024-01398-y.
35 L.-H. Xu, Q.-D. Ou, Y.-Q. Li, Y.-B. Zhang, X.-D. Zhao, H.-Y. Xiang, J.-D. Chen, L. Zhou, S.-T. Lee and J.-X. Tang, *ACS Nano*, 2015, **10**, 5b07302, DOI: 10.1021/acsnano.5b07302.
36 Y. Li, M. Kovacic, J. Westphalen, S. Oswald, Z. Ma, C. Hanisch, P.-A. Will, L. Jiang, M. Junghaehnel, R. Scholz, S. Lenk and S. Reineke, *Nat. Commun.*, 2019, **10**, 2972, DOI: 10.1038/s41467-019-11032-z.
37 J. Song, K.-H. Kim, E. Kim, C.-K. Moon, Y.-H. Kim, J.-J. Kim and S. Yoo, *Nat. Commun.*, 2018, **9**, 3207, DOI: 10.1038/s41467-018-05671-x.
38 L. Suhyeon, D. Hahm, S.-Y. Yoon, H. Yang, W. K. Bae and J. Kwak, *Nano. Res.*, 2022, **15**, 6477, DOI: 10.1007/s12274-022-4204-y.
39 I. G. Jang, V. Murugadoss, T. H. Park, K. R. Son, H. J. Lee, W. Q. Ren, M. J. Yu and T. G. Kim, *Nano-Micro Lett.*, 2022, **14**, 60, DOI: 10.1007/s40820-022-00802-y.
40 M. Mamada and C. Adachi, *Appl. Phys. Lett.*, 2022, **121**, 131103, DOI: 10.1063/5.0100373.
41 J. J. Yang, D. Hu, F. Zhu, Y. Ma and D. Yan, *Sci. Adv.*, 2022, **8**, 50, DOI: 10.1126/sciadv.add1757.
42 L.-X. Wang, C. G. Tang, Z.-S. Tan, H.-Y. Phua, J. Chen, W. Lei, R.-Q. Png, L.-L. Chua and P. K. H. Ho, *Mater. Horiz.*, 2022, **9**, 2147, DOI: 10.1039/d1mh00859e.
43 Y. Kim, T. Lee, B. Chun, J. Kim and J. Kwak, *ACS Photonics*, 2025, **12**, 3840, DOI: 10.1021/acsphotonics.5c00865.
44 M. J. Enright, D. Jasrasaria, M. M. Hanchard, D. R. Needell, M. E. Phelan, D. Weinberg, B. E. McDowell, H.-W. Hsiao, H. Akbari, M. Kottwitz, M. M. Potter, J. Wong, J.-M. Zuo, H. A. Atwater, E. Rabani and R. G. Nuzzo, *J. Phys. Chem. C*, 2022, **126**, 7576, DOI: 10.1021/acs.jpcc.2c01499.
45 B.-C. Liu, J. Bao, W. He, Y.-M. Xie, Q. Lin, B. Song, S.-Q. Sun, Q. Sun, X. Peng, X. Chen, Y. Li, S.-T. Lee and M.-K. Fung, *Nano Energy*, 2025, **140**, 110982, DOI: 10.1016/j.nanoen.2025.110982.
46 J. Lim, W. K. Bae, D. Lee, M. K. Nam, J. Jung, C. Lee, K. Char and S. Lee, *Chem. Mater.*, 2011, **23**, 4459, DOI: 10.1021/cm201550w.
47 G. O. Eren, S. Sadeghi, H. B. Jalali, M. Ritter, M. Han, I. Baylam, R. Melikov, A. Onal, F. Oz, M. Sahin, C. W. Ow-Yang, A. Sennaroglu, R. T. Lechner and S. Nizamoglu, *ACS Appl. Mater. Interfaces*, 2021, **13**, 32022, DOI: 10.1021/acsami.1c08118.
48 M. Nam, J. Chang, H. Kim, Y. H. Son, Y. Jeon, J. H. Kwon and K. C. Choi, *npj Flexible Electron.*, 2024, **8**, 17, DOI: 10.1038/s41528-024-00303-5.
49 H. Song, G. Luo, Z. Ji, R. Bo, Z. Xue, D. Yan, F. Zhang, K. Bai, J. Liu, X. Cheng, W. Pang, Z. Shen and Y. Zhang, *Sci. Adv.*, 2022, **8**, eabm3785, DOI: 10.1126/sciadv.abm3785.
50 M. Miyakawa, H. Tsuji, T. Takei, T. Yamamoto, Y. Fujisaki and M. Nakata, *Adv. Electron. Mater.*, 2024, **11**, 2400676, DOI: 10.1002/aelm.202400676.
51 H. Lee, D. Ko and C. Lee, *ACS Appl. Mater. Interfaces*, 2019, **11**, 11667, DOI: 10.1021/acsami.8b22217.
52 H. Ryu, D. Shin, B. Yoon, W. K. Bae, J. Kwak and H. Lee, *ACS Appl. Mater. Interfaces*, 2025, **17**, 1408, DOI: 10.1021/acsami.4c12250.
53 I.-H. Park, S. E. Lee, Y. Kim, S. Y. You, Y. K. Kim and G.-T. Kim, *Org. Electron.*, 2022, **101**, 106404, DOI: 10.1016/j.orgel.2021.106404.
54 B. N. Pal, Y. Ghosh, S. Brovelli, R. Laocharoensuk, V. I. Klimov, J. A. Hollingsworth and H. Htoon, *Nano Lett.*, 2012, **12**, 331, DOI: 10.1021/nl203620f.
55 Z. Chen, Q. Su, Z. Qin and S. Chen, *Nano Res.*, 2020, **14**, 1, DOI: 10.1007/s12274-020-3091-3.
56 F. Krieg, S. T. Ochsenbein, S. Yakunin, S. ten Brinck, P. Aellen, A. Suess, B. Clerc, D. Guggisberg, O. Nazarenko, Y. Shynkarenko, S. Kumar, C.-J. Shih, I. Infante and M. V. Kovalenko, *ACS Energy Lett.*, 2018, **3**, 641, DOI: 10.1021/acsenergylett.8b00035.
57 D. S. Chung, T. Davidson-Hall, G. Cotella, Q. Lyu, P. Chun and H. Aziz, *Nano-Micro Lett.*, 2022, **14**, 212, DOI: 10.1007/s40820-022-00970-x.
58 G. Almeida, L. van der Poll, W. H. Evers, E. Szoboszlai, S. J. W. Vonk, F. T. Rabouw and A. J. Houtepen, *Nano Lett.*, 2023, **23**, 8697, DOI: 10.1021/acs.nanolett.3c02630.
59 D. Jung, J. W. Park, S. Min, H. J. Lee, J. S. Park, G.-M. Kim, D. Shin, S. Im, J. Lim, K. H. Kim, J. A. Chae, D. C. Lee, R. Pugin, X. Bulliard, E. Hwang, J.-S. Park, Y.-S. Park and W. K. Bae, *Nat. Commun.*, 2024, **15**, 5561, DOI: 10.1038/s41467-024-49791-z.
60 H. Li, J. Zhang, W. Wen, Y. Zhao, H. Gao, B. Ji, Y. Wang, L. Jiang and Y. Wu, *Nat. Commun.*, 2025, **16**, 4257, DOI: 10.1038/s41467-025-59527-2.
61 Y. Bi, J. Sun, S. Cao, Q. Li, J. Zheng, X. Yuan, Y. Wang, B. Zou and J. Zhao, *Nat. Commun.*, 2025, **16**, 1945, DOI: 10.1038/s41467-025-57304-9.
62 C.-T. Li and H.-S. Chen, *ACS Appl. Nano Mater.*, 2024, **7**, 8258, DOI: 10.1021/acsanm.4c01052.
63 Z. Hu, Y. Yin, M. U. Ali, W. Peng, S. Zhang, D. Li, T. Zou, Y. Li, S. Jiao, S.-J. Chen, C.-Y. Lee, H. Meng and H. Zhou, *Nanoscale*, 2020, **12**, 2103, DOI: 10.1039/C9NR09086J.
64 V. Wood, M. J. Panzer, J. E. Halpert, J.-M. Caruge, M. G. Bawendi and V. Bulovic, *ACS Nano*, 2009, **3**, 3581, DOI: 10.1021/nn901074r.
65 Q. Su, Z. Chen and S. Chen, *Nat. Commun.*, 2024, **15**, 8150, DOI: 10.1038/s41467-024-52521-0.
66 W. Zhang, B. Li, C. Chang, F. Chen and H. Shen, *Nat. Commun.*, 2024, **15**, 783, DOI: 10.1038/s41467-024-44894-z.
67 Y. Liu, Y. Sun, X. Yan, Q. Lin and H. Shen, *Light: Sci. Appl.*, 2025, **14**, 50, DOI: 10.1038/s41377-024-01727-4.
68 D. Jung, J. W. Park, S. Min, H. J. Lee, J. S. Park, G.-M. Kim, D. Shin, S. Im, J. Lim, K. H. Kim, J. A. Chae, D. C. Lee, R. Pugin, X. Bulliard, E. Hwang, J.-S. Park, Y.-S. Park and W. K. Bae, *Nat. Commun.*, 2024, **15**, 5561, DOI: 10.1038/s41467-024-49791-z.
69 H. Baek, S. Kang, J. Heo, S. Choi, R. Kim, K. Kim, N. Ahn, Y.-G. Yoon, T. Lee, J. B. Chang, K. S. Lee, Y.-G. Park and

J. Park, *Nat. Commun.*, 2024, **15**, 1671, DOI: 10.1038/s41467-024-45944-2.
70 W. K. Bae, Y.-S. Park, J. Lim, D. Lee, L. A. Padilha, H. McDaniel, I. Robel, C. Lee, J. M. Pietryga and V. I. Klimov, *Nat. Commun.*, 2013, **4**, 2661, DOI: 10.1038/ncomms3661.
71 W. K. Bae, L. A. Padilha, Y.-S. Park, H. McDaniel, I. Robel, J. M. Pietryga and V. I. Klimov, *ACS Nano*, 2013, **7**, 3411, DOI: 10.1021/nn4002825.
72 J. Lim, B. G. Jeong, M. Park, J. K. Kim, J. M. Pietryga, Y.-S. Park, V. I. Klimov, C. Lee, D. C. Lee and W. K. Bae, *Adv. Mater.*, 2014, **26**, 8034, DOI: 10.1002/adma.201403620.
73 K.-Y. Lai, S. Yang, T.-C. Tsai, I.-A. Yao, C.-L. Yang, C.-C. Chang and H.-S. Chen, *Nanomaterials*, 2022, **4**, 2683, DOI: 10.3390/nano12152683.
74 Y. Chen, J. Cai, J. Lin, X. Hu, C. Wang, E. Chen, J. Sun, Q. Yan and T. Guo, *Opt. Lett.*, 2022, **47**, 166, DOI: 10.1364/OL.446231.
75 C.-Y. Cheng and M.-H. Mao, *J. Appl. Phys.*, 2016, **120**, 083103, DOI: 10.1063/1.4961425.
76 M. Palei, V. Caligiuri, S. Kudera and R. Krahne, *ACS Appl. Mater. Interfaces*, 2018, **10**, 22356, DOI: 10.1021/acsami.8b03769.
77 J. Du, Y. Huang, Y. Yun, W. Wei, S. Jiang, Y. Yang, M. Chen and C. Li, *Appl. Surf. Sci.*, 2025, **700**, 163205, DOI: 10.1016/j.apsusc.2025.163205.
78 W. B. Gunnarsson, Z. Xu, N. K. Noel and B. P. Rand, *ACS Appl. Mater. Interfaces*, 2022, **14**, 34247, DOI: 10.1021/acsami.2c00860.
79 S. Geng, Y. Wen, B. Zhou, Z. Wang, Z. Wang, P. Wang, Y. Jing, K. Cao, K. Wang and R. Chen, *ACS Appl. Electron. Mater.*, 2021, **3**, 2362, DOI: 10.1021/acsaelm.1c00243.
80 T. Ding, Y.-M. Song, M.-W. Wang, H. Liu, J. Jiang, J.-C. Xu, H.-C. Liu, K.-W. Ng and S.-P. Wang, *J. Phys. Chem. Lett.*, 2024, **15**, 9233, DOI: 10.1021/acs.jpclett.4c01974.
81 R. D. Schaller and V. I. Klimov, *Phys. Rev. Lett.*, 2004, **92**, 186601, DOI: 10.1103/PhysRevLett.92.186601.
82 R. J. Ellingson, M. C. Beard, J. C. Johnson, P. Yu, O. I. Micic, A. J. Nozik, A. Shabaev and A. L. Efros, *Nano Lett.*, 2005, **5**, 865, DOI: 10.1021/nl0502672.
83 W. A. Tisdale, K. J. Williams, B. A. Timp, D. J. Norris, E. S. Aydil and X.-Y. Zhu, *Science*, 2010, **328**, 1547, DOI: 10.1126/science.1185509.
84 O. E. Semonin, J. M. Luther, S. Choi, H.-Y. Chen, G. Gao, A. J. Nozik and M. C. Beard, *Science*, 2011, **334**, 1530, DOI: 10.1126/science.1209845.
85 G. Ba, Q. Xu, X. Li, Q. Lin, H. Shen and Z. Du, *Opt. Express*, 2021, **29**, 12169, DOI: 10.1364/OE.421029.
86 R. Takahashi, T. Dazai, Y. Tsukahara, A. Borowiak and H. Koinuma, *J. Appl. Phys.*, 2022, **131**, 175302, DOI: 10.1063/5.0087044.
87 H. H. Kim, S. Park, Y. Yi, D. I. Son, C. Park, D. K. Hwang and W. K. Choi, *Sci. Rep.*, 2015, **5**, 8968, DOI: 10.1038/srep08968.
88 M. Kim, J. Kim, J. Cho, H. Kim, N. Lee and B. Choi, *Mater. Res. Bull.*, 2016, **82**, 115, DOI: 10.1016/j.materresbull.2016.03.008.
89 Y. Guo and J. Robertson, *Appl. Phys. Lett.*, 2014, **105**, 222110, DOI: 10.1063/1.4903538.
90 W. Xu, Q. Hu, S. Bai, C. Bao, Y. Miao, Z. Yuan, T. Borzda, A. J. Barker, E. Tyukalova, Z. Hu, M. Kawecki, H. Wang, Z. Yan, X. Liu, X. Shi, K. Uvdal, M. Fahlman, W. Zhang, M. Duchamp, J.-M. Liu, A. Petrozza, J. Wang, L.-M. Liu, W. Huang and F. Gao, *Nat. Photonics*, 2019, **13**, 418, DOI: 10.1038/s41566-019-0390-x.
91 T. Scharff, W. Ratzke, J. Zipfel, P. Klemm, S. Bange and J. M. Lupton, *Nat. Commun.*, 2021, **12**, 2071, DOI: 10.1038/s41467-021-22191-3.
92 Y.-H. Kim, S. Kim, A. Kakekhani, J. Park, J. Park, Y.-H. Lee, H. Xu, S. Nagane, R. B. Wexler, D.-H. Kim, S. H. Jo, L. Martínez-Sarti, P. Tan, A. Sadhanala, G.-S. Park, Y.-W. Kim, B. Hu, H. J. Bolink, S. Yoo, R. H. Friend, A. M. Rappe and T.-W. Lee, *Nat. Photonics*, 2021, **15**, 148, DOI: 10.1038/s41566-020-00732-4.
93 X. Zhu, X. Luo, Y. Deng, H. Wei, F. Peng, L. Ying, F. Huang, Y. Hu and Y. Jin, *Sci. Adv.*, 2024, **10**, 33, DOI: 10.1126/sciadv.ado0614.
94 H. G. Lee, Y. W. Kwon, W. H. Jung, H. Lee, M. S. Kim, H.-M. Kim, H. Kim, H. J. Kim, D. C. Lee, J. Lim and S.-Y. Cho, *ACS Appl. Mater. Interfaces*, 2025, **17**, 3597, DOI: 10.1021/acsami.4c17722.
95 S. Lee, C.-Y. Han, A. Hong, J. Kim, H. Yang, B. J. Jung and J. Kwak, *Semicond. Sci. Technol.*, 2019, **34**, 085002, DOI: 10.1088/1361-6641/ab2b52.
96 Z. Tang, J. Lin, L. Wang, Y. Lv, Y. Hu, Y. Fan, X. Guo, J. Zhao, Y. Wang and X. Liu, *J. Mater. Chem. C*, 2017, **5**, 9138, DOI: 10.1039/C7TC02897K.
97 H. Kim, J.-H. Youn, G. Seo and J. Jang, *J. Mater. Chem. C*, 2013, **1**, 1567, DOI: 10.1039/C2TC00339B.
98 H. Li, S. Zhou and S. Chen, *Laser Photonics Rev.*, 2023, **17**, 2300371, DOI: 10.1002/lpor.202300371.
99 Y. Yang, Y. Zheng, W. Cao, A. Titov, J. Hyvonen, J. R. Manders, J. Xue, P. H. Holloway and L. Qian, *Nat. Photonics*, 2015, **9**, 259, DOI: 10.1038/nphoton.2015.36.
100 H. Shen, Q. Gao, Y. Zhang, Y. Lin, Q. Lin, Z. Li, L. Chen, Z. Zeng, X. Li, Y. Jia, S. Wang, Z. Du, L. S. Li and Z. Zhang, *Nat. Photonics*, 2019, **13**, 192, DOI: 10.1038/s41566-019-0364-z.
101 X. Yang, K. Dev, J. Wang, E. Mutlugun, C. Dang, Y. Zhao, S. Liu, Y. Tang, S. T. Tan, X. W. Sun and H. V. Demir, *Adv. Funct. Mater.*, 2014, **24**, 5977, DOI: 10.1002/adfm.201400190.
102 H. Li, F. Tian and S. Chen, *Nano Res.*, 2023, **16**, 10156, DOI: 10.1007/s12274-023-5520-6.
103 Y. Zhu, R. Xu, Y. Zhou, Z. Xu, Y. Liu, F. Tian, X. Zheng, F. Ma, R. Alsharafi, H. Hu, T. Guo, T. W. Kim and F. Li, *Adv. Opt. Mater.*, 2020, **8**, 2001479, DOI: 10.1002/adom.202001479.
104 L. Shi and S. Chen, *ACS Appl. Mater. Interfaces*, 2022, **14**, 30039, DOI: 10.1021/acsami.2c06670.
105 T. Lee, B. J. Kim, H. Lee, D. Hahm, W. K. Bae, J. Lim and J. Kwak, *Adv. Mater.*, 2022, **34**, 2106276, DOI: 10.1002/adma.202106276.

106 H. Yu, H. Zhu, M. Xu, J. Zhang, H. Feng, L. Zhang, S. Liu and W. Xie, *ACS Photonics*, 2023, **10**, 2192, DOI: 10.1021/acsphotonics.2c00863.
107 G. Liu, X. Zhou and S. Chen, *ACS Appl. Mater. Interfaces*, 2016, **8**, 16768, DOI: 10.1021/acsami.6b03367.
108 M. Li, R. Li, L. Wu, X. Lin, X. Xia, Z. Ao, X. Sun, X. Chen and S. Chen, *Nat. Commun.*, 2024, **15**, 5161, DOI: 10.1038/s41467-024-49574-6.
109 Y. Jeon, S. Sim, D. Shin, W. K. Bae, H. Lee and H. Lee, *Adv. Electron. Mater.*, 2024, **10**, 2400195, DOI: 10.1002/aelm.202400195.
110 F. Tian, T. Zhou, X. Zhang, R. Chen and S. Chen, *Light: Sci. Appl.*, 2025, **14**, 279, DOI: 10.1038/s41377-025-01972-1.
111 T.-W. Lee, D. Kim, J. H. Han, S. Lee, H. Lee, S. Choi and K. C. Choi, *Photonics Res.*, 2021, **9**, 1784, DOI: 10.1364/PRJ.418160.
112 D.-Y. Hyeong and H. Lee, *J. Inf. Disp.*, 2025, **26**, 437, DOI: 10.1080/15980316.2025.2539677.
113 W. Wang, Z. Wu, G. Mei, J. Ma, H. An, K. Wang, X. W. Sun and Z. Peng, *J. Mater. Chem. C*, 2024, **12**, 1668, DOI: 10.1039/D3TC03780K.
114 G. Mei, K. Wang and X. W. Sun, *Nat. Nanotechnol.*, 2024, **19**, 1427, DOI: 10.1038/s41565-024-01709-y.
115 E. S. Lee, R. K. Jha, E. A. Kim, H. Ban, N. Kwak, N. Oh, H. Kim and S.-Y. Cho, *Adv. Opt. Mater.*, 2025, e03102, DOI: 10.1002/adom.202503102.
116 Y. Miao, L. Cheng, W. Zou, L. Gu, J. Zhang, Q. Guo, Q. Peng, M. Xu, Y. He, S. Zhang, Y. Cao, R. Li, N. Wang, W. Huang and J. Wang, *Light: Sci. Appl.*, 2020, **9**, 89, DOI: 10.1038/s41377-020-0328-6.
117 L. Zhao, K. M. Lee, K. Roh, S. U. Z. Khan and B. P. Rand, *Adv. Mater.*, 2019, **31**, 1805836, DOI: 10.1002/adma.201805836.
118 G. Mei, X. Xiao, S. Ahmad, H. Lin, Y. Tan, K. Wang, X. W. Sun and W. C. H. Choy, *Adv. Opt. Mater.*, 2023, **11**, 2300912, DOI: 10.1002/adom.202300912.
119 C. Xiang, W. Koo, F. So, H. Sasabe and J. Kido, *Light: Sci. Appl.*, 2013, **2**, e74, DOI: 10.1038/lsa.2013.30.
120 L. Chen, Z. Qin and S. Chen, *Small Methods*, 2022, **6**, 2101090, DOI: 10.1002/smtd.202101090.
121 G. Mei, W. Wang, D. Wu, P. A. Surman, K. Wang, W. C. H. Choy, X. Yang, W. Xu and X. W. Sun, *IEEE Photonics J.*, 2022, **14**, 8219709, DOI: 10.1109/JPHOT.2022.3159278.
122 J. Lee, S. Hofmann, M. Furno, Y. H. Kim, J.-I. Lee, H. Y. Chu, B. Lüssem and K. Leo, *Opt. Lett.*, 2012, **37**, 2007, DOI: 10.1364/OL.37.002007.
123 H. Kim and S.-Y. Cho, *J. Inf. Disp., arXiv*, in press, 2026, DOI: 10.48550/arXiv.2503.13924.
124 H. Kim and S.-Y. Cho, *Opt. Express*, 2025, **33**, 43931, DOI: 10.1364/OE.572218.
125 C. Dong, X. Fu, L. Cao, S. Amoah, K. Gundogdu, J. Li and F. So, *ACS Appl. Mater. Interfaces*, 2020, **12**, 31667, DOI: 10.1021/acsami.0c05825.
126 T. Lee, D. Hahm, K. Kim, W. K. Bae, C. Lee and J. Kwak, *Small*, 2019, **15**, e1905162, DOI: 10.1002/smll.201905162.
127 D. Li, J. Feng, Y. Zhu, Z. Lu, C. Pei, Z. Chen, Y. Li, X. Li and X. Xu, *Nano Res.*, 2021, **14**, 4243, DOI: 10.1007/s12274-021-3596-4.
128 H. Benisty, H. D. Neve and C. Weisbuch, *IEEE J. Quantum Electron.*, 1998, **34**, 1612, DOI: 10.1109/3.709578.
129 M. Gryga, D. Ciprian and P. Hlubina, *Sensors*, 2022, **22**, 3627, DOI: 10.3390/S22103627.
130 B. Gao, J. P. George, J. Beeckman and K. Neyts, *Opt. Express*, 2020, **28**, 12837, DOI: 10.1364/OE.391080.
131 A. Mischok, B. Siegmund, F. L. Roux, S. Hillebrandt, K. Vandewal and M. C. Gather, *Nat. Commun.*, 2024, **15**, 10529, DOI: 10.1038/s41467-024-54623-1.
132 H. F. Wittmann, J. Grüner, R. H. Friend, G. W. C. Spencer, S. C. Moratti and A. B. Holmes, *Adv. Mater.*, 1995, **7**, 541, DOI: 10.1002/adma.19950070604.
133 J. C. Loy, W. Qiu, D. Yang, J. Scherlag, J. Scott and B. P. Rand, *Adv. Opt. Mater.*, 2025, **13**, 2402623, DOI: 10.0002/adom.202402623.
134 M. Furno, R. Meerheim, S. Hofmann, B. Lüssem and K. Leo, *Phys. Rev. B:Condens. Matter Mater. Phys.*, 2012, **85**, 115205, DOI: 10.1103/PhysRevB.85.115205.
135 J. Chen, P. Ma, W. Chen and Z. Xiao, *Nano Lett.*, 2021, **21**, 8426, DOI: 10.1021/acs.nanolett.1c03035.
136 C. Liu, B. Li and M. Qiu, *Adv. Devices Instrum.*, 2024, **5**, 0045, DOI: 10.34133/adi.0045.
137 H. Xu, J. Song, P. Zhou, Y. Song, J. Xu, H. Shen, S. Fang, Y. Gao, Z. Zuo, J. M. Pina, O. Voznyy, C. Yang, Y. Hu, J. Li, J. Du, E. H. Sargent and F. Fan, *Nat. Photonics*, 2024, **18**, 186, DOI: 10.1038/s41566-023-01344-4.
138 S. Kumar, T. Marcato, F. Krumeich, Y.-T. Li, Y.-C. Chiu and C.-J. Shih, *Nat. Commun.*, 2022, **13**, 2106, DOI: 10.1038/s41467-022-29812-5.
139 Q. Zhang, X. Gu, Z. Chen, J. Jiang, Z. Zhang, J. Wei, F. Li, X. Jin, Y. Song and Q. Li, *Opt. Express*, 2017, **25**, 17683, DOI: 10.1364/OE.25.017683.
140 T. Lee, M. Lee, K. Kim, H. Lee, S.-Y. Yoon, H. Yang, S. Yu and J. Kwak, *Adv. Opt. Mater.*, 2024, **12**, 2302509, DOI: 10.1002/adom.202302509.
141 Y. Y. Kim, J. J. Park, S. J. Ye, W. J. Hyun, H.-G. Im, B.-S. Bae and O. O. Park, *RSC Adv.*, 2016, **6**, 65450, DOI: 10.1039/c6ra12718e.
142 I. Son and J. H. Lee, *ACS Appl. Mater. Interfaces*, 2020, **12**, 30862, DOI: 10.1021/acsami.0c08730.
143 P. Spinelli, M. A. Verschuuren and A. Polman, *Nat. Commun.*, 2012, **3**, 692, DOI: 10.1038/ncomms1691.
144 Y. Zhao, B. Xu, Z. Duan, A. Wang, H. Qi, S. Wang and B. Hu, *J. Lumin.*, 2025, **277**, 120959, DOI: 10.1016/j.jlumin.2024.120959.
145 S. Park, S. Sim, H. Lee, H. J. Lee, J. W. Park, J. S. Park, W. K. Bae and H. Lee, *Micro Nano Eng.*, 2025, 100325, DOI: 10.1016/j.mne.2025.100325.
146 P. Guo, Y. Xie, P. Yuan, S. Li, Y. Guo, W. Jin, J. Song, K. Zhang and H. Qi, *Phys. Status Solidi RRL*, 2025, **19**, 2400353, DOI: 10.1002/pssr.202400353.
147 D. Zhang and J. Xu, *Opt. Lett.*, 2020, **45**, 2243, DOI: 10.1364/OL.390266.

148 S. Yeom, H. Kim, K. Kim, C. W. Joo, H. Cho, H. Cho, S. Choi, W. J. Lee, Y. S. Jung, B.-H. Kwon and J.-H. Na, *Opt. Express*, 2020, **28**, 26519, DOI: 10.1364/OE.401328.
149 Y. Jia, H. Li, N. Guo, F. Li, T. Li, H. Ma, Y. Zhao, H. Gao, D. Wang, J. Feng, Z. He, L. Jiang and Y. Wu, *Nat. Commun.*, 2025, **16**, 7643, DOI: 10.1038/s41467-025-62345-1.
150 T. Lee, M. Kim, B. Chun, G. Park, S. Yim, S. Yu and J. Kwak, *ACS Photonics*, 2024, **11**, 5050, DOI: 10.1021/acsphotonics.4c01617.
151 J. Y. Park, B. J. Kim, C. J. Yoo, W. J. Dong, I. Lee, S. Kim and J.-L. Lee, *Sci. Rep.*, 2020, **10**, 5540, DOI: 10.1038/s41598-020-62257-8.
152 Z. Liu, F. Li, G. Huang, J. Wei, G. Jiang and Y. Huang, *J. Nanomater.*, 2020, **1**, 8858996, DOI: 10.1155/2020/8858996.
153 S. Wang, C. Li, Y. Xiang, H. Qi, Y. Fang, A. Wang, H. Shen and Z. Du, *Nanoscale Adv.*, 2020, **2**, 1967, DOI: 10.1039/d0na00150c.
154 K. Kang, S. Im, C. Lee, J. Kim and D. Kim, *Sci. Rep.*, 2021, **29**, 9232, DOI: 10.1038/s41598-021-88641-6.
155 S. Chen, W. Cao, T. Liu, S.-W. Tsang, Y. Yang, X. Yan and L. Qian, *Nat. Commun.*, 2019, **10**, 765, DOI: 10.1038/s41467-019-08749-2.